Novel Electrochemical Packed-Bed Reactor for Carbon Dioxide Reduction

Mr. Suwakul Chaiwarit

เครื่องปฏิกรณ์ไฟฟ้าเคมีชนิดเบดแบบใหม่สำหรับการรีดิวซ์คาร์บอนไดออกไซด์

นายสุวกุล ชัยวาฤทธิ์

Thesis Title	Novel Electrochemical Packed-Bed Reactor for Carbon Dioxide Reduction
By	Mr. Suwakul Chaiwarit
Field of Study	Chemical Engineering
Thesis Advisor	Assistant Professor PALANG BUMROONGSAKULSAWAT

Accepted by the FACULTY OF ENGINEERING, Chulalongkorn University in Partial Fulfillment of the Requirement for the Master of Engineering

.... Dean of the FACULTY OF ENGINEERING
(Professor SUPOT TEACHAVORASINSKUN)

THESIS COMMITTEE

.... Chairman
(Assistant Professor PARAVEE VAS-UMNUAY)

.... Thesis Advisor
(Assistant Professor PALANG BUMROONGSAKULSAWAT)

.... Examiner
(Doctor SUPAREAK PRASERTHDAM)

.... External Examiner
(Assistant Professor Pornchai Bumroongsri)

จุฬาลงกรณ์มหาวิทยาลัย

CHULALONGKORN UNIVERSITY

สุวกุล ชัยวาฤทธิ์ : เครื่องปฏิกรณ์ไฟฟ้าเคมีชนิดเบดแบบใหม่สำหรับการรีดิวซ์คาร์บอนไดออกไซด์. (Novel Electrochemical Packed-Bed Reactor for Carbon Dioxide Reduction) อ.ที่ปรึกษาหลัก : ผศ. ดร.พลัง บำรุงสกุลสวัสดิ์

การลดก๊าซคาร์บอนไดออกไซด์ (CO_2) ด้วยวิธีทางไฟฟ้าเคมีเป็นหนึ่งในวิธีที่จะสามารถนำ CO_2 มาเพิ่มมูลค่าโดยเปลี่ยน CO_2 เป็นผลิตภัณฑ์เคมีอื่น ๆ อย่างไรก็ตาม การออกแบบอุปกรณ์สำหรับเปลี่ยน CO_2 ด้วยวิธีไฟฟ้าเคมีมักจะออกแบบสแต็ก (Stack) เพื่อเพิ่มอัตราส่วนพื้นผิวต่อปริมาตรให้สูงสุดนั้นต้องใช้ชิ้นส่วนที่ซับซ้อนจำนวนมากในการประกอบ การออกแบบสแต็กสำหรับเทคโนโลยีระดับอุตสาหกรรมในปัจจุบัน ต้องการป้อนสารตั้งต้นให้ผ่านช่องขนาดเล็กตลอดทั่วทั้งเซลล์ ที่มักถูกจำกัดด้วยขนาดเมมเบรนประมาณ 1 ตร.ม. การวิจัยครั้งนี้มีวัตถุประสงค์เพื่อ มุ่งเน้นการพัฒนาเครื่องปฏิกรณ์ไฟฟ้าเคมีชนิดใหม่ที่เหมาะกับการใช้งานในระดับอุตสาหกรรมสำหรับการรีดิวซ์ก๊าซCO_2 เป็น ก๊าซ CO โดยส่วนประกอบของเซลล์สำหรับเครื่องปฏิกรณ์ไฟฟ้าเคมีชนิดใหม่ชนิดเบดนิ่งประกอบด้วย ซิงค์ ดิพอสซิท เฟลทฺ (Zn deposited felt), เรซินแลกเปลี่ยนไอออน (Ion exchange resin)และไททาเนียมเคลือบทองคำขาว (Platinized titanium) เรียงตามลำดับดังที่กล่าวมาข้างต้น ก๊าซ CO_2 ที่มีความชื้นถูกป้อนเข้าสู่เครื่องปฏิกรณ์ที่มีการจ่ายแรงดันไฟฟ้า (Applied voltage) แก่กับเครื่องปฏิกรณ์ไฟฟ้าเคมีชนิดใหม่ชนิดเบดนิ่งในขณะเดียวกัน เพื่อเริ่มต้นปฏิกิริยารีดิวซ์ก๊าซ CO_2 การวิจัยครั้งนี้ศึกษาผลของแรงดันไฟฟ้าที่ให้แก่เครื่องปฏิกรณ์ไฟฟ้าเคมีชนิดใหม่ชนิดเบดนิ่งที่ 3 ถึง 6 โวลต์ สำหรับเบดนิ่งแบบหนึ่งเซลล์ 1 เซลล์ และ 8 ถึง 11 โวลต์ สำหรับเบดนิ่งแบบหนึ่งเซลล์ 2 เซลล์ และผลของอัตราการไหลของ CO_2 ที่ 40, 80 และ 120 มิลลิลิตรต่อนาทีต่อประสิทธิภาพการรีดิวซ์ ก๊าซ CO_2 เป็น ก๊าซ CO ความเข้มข้นของ CO ที่ออกจากเครื่องปฏิกรณ์ไฟฟ้าเคมีชนิดใหม่ชนิดเบดนิ่งวิเคราะห์ด้วยอินฟราเรดสเปกโทรสโกปีแบบออนไลน์ จากผลการวิจัยพบว่าการเพิ่มขึ้นของความเข้มข้นของ CO (CO concentration) และกระแสไฟ (Current) สอดคล้องกับแรงดันไฟฟ้าที่เพิ่มขึ้น สำหรับเบดนิ่งแบบ 1 เซลล์ การผลิต CO และประสิทธิภาพทางไฟฟ้า (Faradaic efficiency) ที่สูงสุดเกิดขึ้นเมื่อจ่ายแรงดันไฟฟ้า 6 โวลต์ และใช้อัตราการไหลที่ 80 มิลลิลิตรต่อนาทีส่วนสภาวะที่เหมาะสมที่สุดสำหรับเบดนิ่งแบบ 2 เซลล์อยู่ที่ 11 โวลต์ และ 120 มิลลิลิตรต่อนาที อย่างไรก็ตาม ผลของอัตราการไหลของ CO_2 อาจขัดแย้งต่อการถ่ายเทมวลเมื่ออัตราการไหลสูง ผลจากการวิเคราะห์ CO ที่เกิดขึ้นยืนยันว่าเครื่องปฏิกรณ์ไฟฟ้าเคมีชนิดใหม่ชนิดเบดนิ่งสามารถรีดิวซ์ก๊าซ CO_2 เป็น ก๊าซ CO ได้

จุฬาลงกรณ์มหาวิทยาลัย
CHULALONGKORN UNIVERSITY

สาขาวิชา	วิศวกรรมเคมี	ลายมือชื่อนิสิต ....
ปีการศึกษา	2563	ลายมือชื่อ อ.ที่ปรึกษาหลัก ....

6170316621 : MAJOR CHEMICAL ENGINEERING
KEYWORD: CO2, Electrochemical reduction, Packed bed reactor, Fixed bed reactor

Suwakul Chaiwarit : Novel Electrochemical Packed-Bed Reactor for Carbon Dioxide Reduction. Advisor: Asst. Prof. PALANG BUMROONGSAKULSAWAT

Electrochemical reduction of carbon dioxide (CO_2) is a promising strategy to recycle CO_2 into valuable chemical products. Nevertheless, a conventional apparatus which usually utilizes stack design to maximize its surface-to-volume ratio requires many elements and complicated instruction assembly. The stack design often requires feed streams to flow in narrow channels throughout the cell, which is also constrained by membrane size roughly 1 m^2 by current manufacture technology. This research focuses on development of a new type of electrochemical reactor that is suitable for industrial-scale applications. The novel electrochemical packed-bed reactor is designed for the electroreduction to covert CO_2 into CO in the gas phase. Humidified CO_2 was fed through the reactor, and a voltage was applied to the bed for initiate electrochemical reactions. The bed consists of 3 compartments including Zinc (Zn) deposited felt, ion-exchange resin, and platinized titanium arranged in this order. Effects of applied voltage and CO_2 flow rates toward the CO_2 reduction performance was investigated. The increasing of CO concentration and current were achieved with increasing voltage. The maximum CO concentation and the highest faradaic efficiency were observed at 6 V and 80 ml min^{-1} for a single-cell bed. The optimal condition for a two-cell bed was 11 V and 120 ml min^{-1}. However, the effects of flow rate might oppose effects of mass transfer at high flow rate. An online infrared spectroscopy was coupled to the novel electrochemical packed-bed reactor for the CO product detection. The CO product analysis confirmed that the novel electrochemical packed-bed reactor successfully converts CO_2 to CO.

จุฬาลงกรณ์มหาวิทยาลัย

CHULALONGKORN UNIVERSITY

Field of Study:	Chemical Engineering	Student's Signature ....
Academic Year:	2020	Advisor's Signature ....

ACKNOWLEDGEMENTS

TABLE OF CONTENTS

Page

จุฬาลงกรณ์มหาวิทยาลัย

CHULALONGKORN UNIVERSITY

List of tables

Page

จุฬาลงกรณ์มหาวิทยาลัย
CHULALONGKORN UNIVERSITY

List of figures

Acronym

Acronym / Symbol	Meaning
AEM	Anion exchange membrane
BPM	Bipolar membrane
CO_2RR	CO_2 reduction reaction
CEM	Cation exchange membrane
FE	Faradaic efficiency
GDE	Gas diffusion electrode
HER	Hydrogen evolution reaction
J	Current density
NHE	Normal hydrogen electrode
PEM	Proton exchange membrane
R	Reaction
RHE	Reversible hydrogen electrode
SCE	Saturated calomel electrode
SOEC	Solid oxide electrolysis cell
SPE	Solid polymer electrolyte
SHE	Standard hydrogen electrode
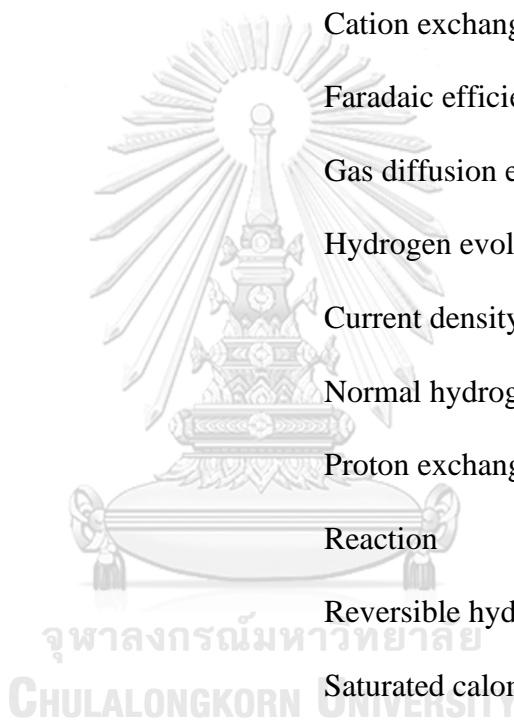
Chapter 1
Introduction

1.1 Background

Fossil fuels have been utilized as a major energy source for a long time. The emission of greenhouse gases from carbon-based energy production combustion increased carbon dioxide (CO_2) concentration in the atmosphere and as a result, accelerated global warming (1). Consequently, the new technologies that minimize CO_2 accumulation and find new energy source has been investigated including storage, capturing, and conversion (2). These strategies have potential to recycle CO_2 into a profitable carbon source. Among them, the conversion of CO_2 is considered as an alternative energy source compared to among technologies because CO_2 can be converted to high energy small molecules such as carbon monoxide (CO) ,and hydrocarbons (3, 4). There are different CO_2 conversion strategies have been studied including electrochemical (5), photochemical (6), and thermochemical (7, 8). Among the other technologies, electrochemical strategies can be operated under ambient temperature and pressure (9). This strategy is also practical to adjust the energy of the active species to reach a high selectivity with precise control of the reaction pathway. Although, electrochemical CO_2 reduction has potential prospect, but its limitations have still to be addressed including the complexity of reduction pathway, high overpotential, and low current density. Thus, electrochemical reduction of CO_2 is vitally developed in catalyst and technology.

For high carbon-based products demands in industry, the selectivity of desire product is typically control by properties of metal electrode. Hori et al. (10) reported the variable selectivity of CO is depends on metal electrodes. To intensify catalytic properties, various methods have been used to improve the reduction performance such as modified surface, nano structuring (11, 12), and so on. However, the CO_2 reduction technologies is far from development to practical application. The CO_2 reduction systems are divided into two categories. The liquid phase system electrochemical reduction systems have been widely developed. However, CO_2 solubility is slightly which hinders CO_2 to interact with catalyst in liquid medium and difficult for scale-up (13). In contrast, electrochemical reduction in gas phase system are arising with the purpose of overcome mass transfer limitations happening in liquid phase and easier reactant mixing, which leads to the possibility to tune the CO_2/steam ratio, and recover product form reactant (14). Regardless, evaluating the performance of numerous electrodes in various electrolytes and different types of cells, at varying process parameters, is challenging.

In recent years, most of the studies focus on improve products selectivity by developed novel electrode, while there are a few attentions in reactors design and scale up. At first, fundamental CO_2 reduction research has been conducted in batch cell (H-cells). Nevertheless, H-cells are drawback because of mass transfer limitations, and low current densities (15). According to H-cells problems, the industries prefer continuous flow reactors which has potential to reduce CO_2. The continuous flow reactors: membrane reactor, micro-reactor, packed-bed reactor have various configurations design in order to overcome reaction limitations. Most of flow cell often design their stack by maximise its surface-to-volume ratio. However, maximising reactor surface-to-volume ratio necessitates many specialized parts and complicated assembly. Consequently, this project aims to develop a new type of electro-chemical reactor that is suitable for industrial-scale applications.

To optimize electrochemical reduction towards CO in flow cells, understanding how the operating parameter (e.g., temperature, pressure, cell potential, flow rate) impact on selectivity of CO production is essential. The novel electrochemical packed-bed reactor is designed for the electro-reduction of CO_2 to CO in the gas phase system. Furthermore, the effect of applied potentials and the influence of CO_2 flow rate were accounted to electrochemical packed-bed reactor performance.

1.2 Objective

1. To develop a novel electrochemical packed-bed reactor for CO_2 reduction in gas phase.
2. To study effects of applied voltages and flow rates on the CO_2 reduction performance.
3. To investigate the performance of a single-cell bed reactor compared to a two-cell bed reactor.

1.3 Scope of study

1. The performance of a single-cell bed and a two-cell bed reactor.
2. The applied voltages from 3 to 6 V for a single-cell bed and 8 to 11 V for a two-cell bed.
3. The flow rates of the CO_2 are 40, 80, and 120 ml min^{-1}.

1.4 Schedule plan

Table 1 Research schedule plan.

No	Activity	Monthly Schedule (2020-2021)								
		July	August	September	October	November	December	January	February	March
1	Literature reviews	■	■	■						
2	Cell and system design		■	■						
3	Preliminary			■	■					
4	Study effect of CO$_2$ flow rate Applied voltage					■	■	■		
5	Gathering information and writing thesis						■	■	■	■

จุฬาลงกรณ์มหาวิทยาลัย

CHULALONGKORN UNIVERSITY

Chapter 2
Theory and Literature reviews

2.1 Theory

2.1.1 Electroreduction of CO_2

Electrochemical reaction is the transformations of substance by shifting of electron. The electrochemical system generally consists of cathode and anode separated by an ion exchange membrane in electrolyte. The membrane acts as a charge carrier and barrier preventing mixing of other products crossing over. During this process, an external power source drives the electron transfer reaction, converting electrical energy to chemical energy of the reaction products. The electrochemical processes have several advantages (i) the reaction is adjustable by electrode potentials; (16) the electrolytes can be recycled and minimized water consumption; (iii) the electric sources in process can be obtain from alternative energy sources; and (iv) the electrochemical process is easy to scale-up.
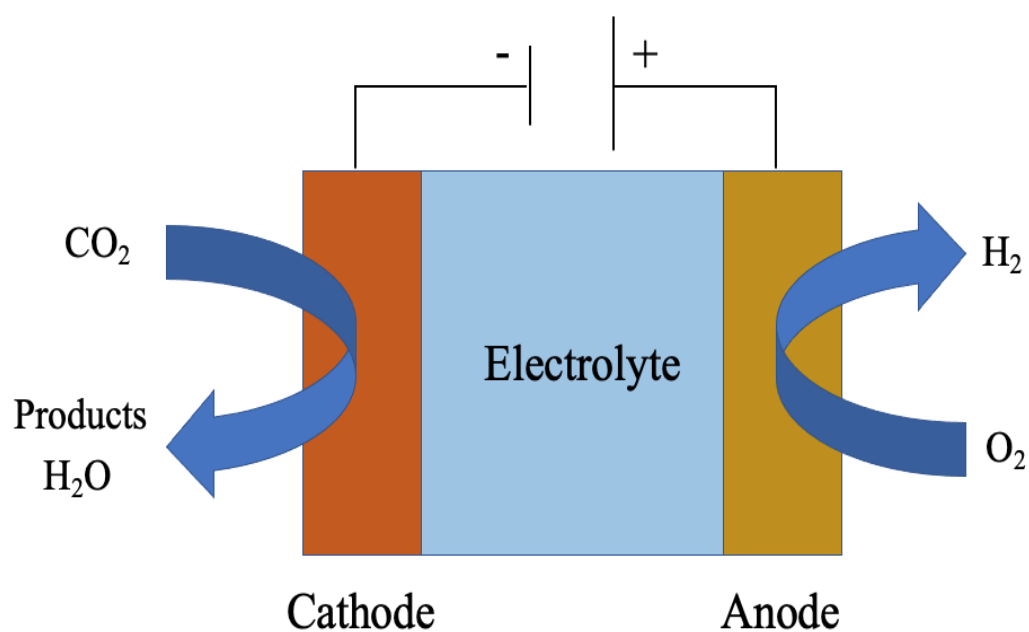
Figure 1 General electrochemical system feature.

In electrochemical carbon dioxide reaction, CO_2 is a linear stable molecule consisting of the oxygen atoms and the carbon atom. CO_2 reduction does not happen simply. Transferring an electron to CO_2 to generate CO_2^- is the rate determining step (RDS) that occur at -1.9V vs SHE because of the high energy barrier is more than the equilibrium value (17). The CO_2 reduction reaction pathway is difficult to control indicated in table 2 (18). Hori and colleagues have been working on CO_2 electroreduction in aqueous solution using different metal electrode and dividing metal electrodes into 4 groups in compliance with the main product (19, 20).

(i)   Pb, Hg, In, Sn, Cd, Tl, and Bi are selective for formic acid production.
(ii)   Au, Ag, Zn, Pd, and Ga produce CO as the major product.
(iii) Cu electrode exhibits an outstanding electrocatalytic activity for multi-hydrocarbon products such as CH_4, C_2H_4 and alcohols, in which CO is formed as an intermediate.
(iv)   Ni, Fe, Pt, and Ti have low electrolytic activity to give production from CO_2 electroreduction, but hydrogen evolution occurs instead.

Nevertheless, the mechanism still needs to be understood further due to the complex synthesis through various type of the materials. In aqueous system, hydrolysis is comparatively positive to rate determining step. Accordingly, hydrogen evolution reaction (HER) favorably competes with CO_2 reduction, and H_2 is the main product (17). The major obstacle preventing conversion of CO_2 is the low solubility of CO_2 in aqueous solution. In addition, the product selectivity of this process can also be enhanced upon various factors, such as electrode potential, electrolyte solution, electrode material, applied voltage, and operating conditions (19,20). The integration of these factors is able to improve CO_2 reduction activities in the liquid phase reactor.

Table 2 Cathodic half–cell reactions in electrochemical CO_2 reduction at pH = 7. (18)

Cathodic half cell reaction	E^0 (V vs. NHE)
$2H^+ + 2e^- \rightarrow H_2$	-0.42
$CO_2 + e^- \rightarrow {}^*CO^-_2$	-1.90
$CO_2 + 2H^+ + 2e^- \rightarrow CO + H_2O$	-0.53
$CO_2 + 2H^+ + 2e^- \rightarrow HCOOH$	-0.61
$CO_2 + 4H^+ + 4e^- \rightarrow HCHO + H_2O$	-0.48
$CO_2 + 6H^+ + 6e^- \rightarrow CH_3OH + H_2O$	-0.38
$CO_2 + 8H^+ + 8e^- \rightarrow CH_4 + H_2O$	-0.24

Despite attempts for increasing the CO_2 reduction performance, the feasible performance is still below the industrial demand. Electroreduction of CO_2 in the gas phase could minimise the drawback of aqueous electrolytes and recover desired product effectively. CO_2 gas flows toward to the cathode directly without liquidise leading to minimise operation cost (21). In addition, gas phase achieves a high current density and overcomes mass transport limitations (22). The key towards the electrochemical CO_2 reduction process is the optimization between the individual cell design and process efficiency.

Table 3 Faradaic efficiencies of the products in CO_2 reduction in 0.1-M TEAP in PC at various metal electrodes at −2.8 V vs. Ag/AgCl/(0.01 M LiCl + 0.1 M TEAP)/PC. quantity of the electric charge: 100. (20)

Electrode	Faradaic efficiency (%)					
	(COOH)$_2$	OHCCOOH	HCOOH	CO	H$_2$	Total
Pb	76.6	2.9	2.5	10.4	0.0	92.4
Cu	0.6	-	-	74.9	0.0	75.5
Ag	1.4	-	2.1	77.4	1.9	82.8
Au	0.2	-	3.7	83.2	13.9	100.9
Zn	0.4	-	-	89.7	0.0	90.1
Pt	1.0	-	7.7	66.6	17.4	92.7

2.1.2 Faradaic efficiency

Faradaic efficiency (FE) or current efficiency implies the selectivity toward a specific product. It is defined as the number of electrons utilized for the desired product formation over the total charge that passed through the cell. The formula for the current efficiency is

$$FE = \frac{ynF}{Q}$$

where y is the number of moles formed of the desired product, n is the number of electrons transferred in the half-cell reaction per mole of product, F is faradaic constant (96,485 C/mol electrons) and Q is the total charge passed between the electrodes (current*time).

2.1.3 Current density

Current density (j or CD) is the total current (I, in Amps) per unit area of the cathode (A/cm^2) calculated by following equation. This parameter describes the reaction rate of a certain product under particular conditions. A greater current density indicates a higher reactant consumption rate.

$$J = \frac{I}{A}$$

Partial current density (j$_{product}$) for a specific product can be calculate by equation below which indicates a generation rate of the specific product.

$$Jproduct = FEproduct \times J$$

2.1.4 CO₂ reduction to CO

The key for improving selectivity of electrochemical CO_2 reduction is CO_2 reactivity on the surface of a metal catalyst. Variety of transition metals have been studied on CO2 electro reduction. The transition metals give different desire product either hydrogen, formic acid or carbon monoxide.

2.1.4.1 Gold (Au)

Gold (Au) is one of useful electrocatalysts for CO_2 reduction to CO. Hori et al. confirmed the CO production from CO_2 on Au electrode. The tefal slope is around 130 mV decade^{-1} in which indicated high partial current density on Au electrode (20). Later, Ikeda et al. investigated electroreduction of CO_2 on Au electrode in phosphate buffer solutions of pH 2 to 6.8. The tefal slope is approximately 120 mV decade^{-1} which agree with Hori's work. This indicates pH does not effect on CO formation at Au electrode, and H_2O act as proton donor not H^+ (23). Eduardus et al. reported CO_2 conversion to CO using nanostructured gold catalysts. The CO faradaic efficiency increased to saturated point of 78% (-0.59 V vs. RHE) as the Au layer increased on carbon paper (24).
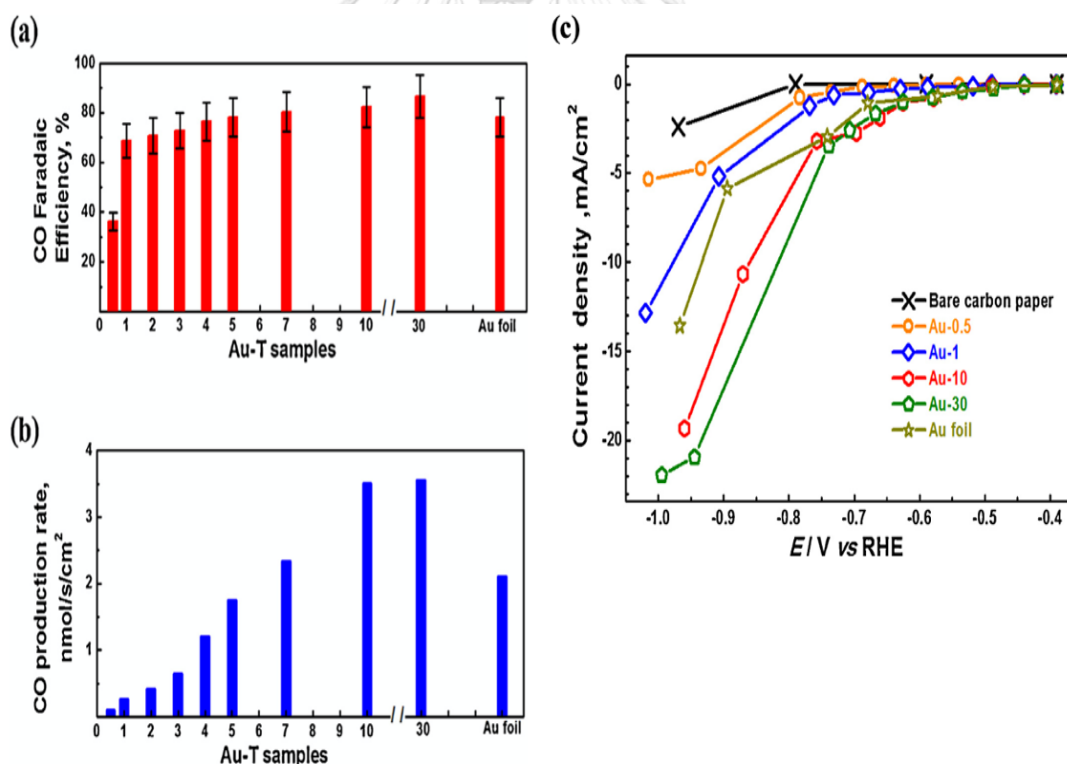
Figure 2 The CO_2 electroreduction performance of Au-T samples and Au foil: (a) CO faradaic efficiencies, (b) CO production rates and (c) total current densities of bare carbon paper, Au-T samples, and Au foil. (24).

2.1.4.2 Silver (Ag)

Silver (Ag) is known as high CO selectivity catalyst. The high CO selectivity of Ag catalysts is because the weak binding energy of both proton and CO on its surfaces, which inhibit HER and CO side reaction (25). The mechanism of CO_2 reduction to CO on silver surface is reported to be responsible via *COOH intermediate. The formation of *COOH possibly happens through a proton-coupled electron transfer (PCET) (R1), or a single electron transfer to form *COO$^-$ (R2, R3) followed by protonation to give *COOH (R4) (26, 27). The schematic of CO_2 reduction to CO mechanism is shown in fig.3 (28).

Proton-coupled electron transfer
$$CO_2(g) + * + H^+(aq) + e^- \rightarrow COOH* \qquad\qquad (R1)$$

Single electron transfer
$$CO(g) + * + e^- \rightarrow COO^-* \qquad\qquad (R2)$$
$$COO^-* + H^+ \rightarrow COOH* \qquad\qquad (R3)$$

*CO and H_2O formation
$$COOH* + H^+(aq) + e^- \rightarrow CO* + H_2O(l) \qquad\qquad (R4)$$

The desorption of CO
$$CO* \rightarrow CO(g) + * \qquad\qquad (R5)$$
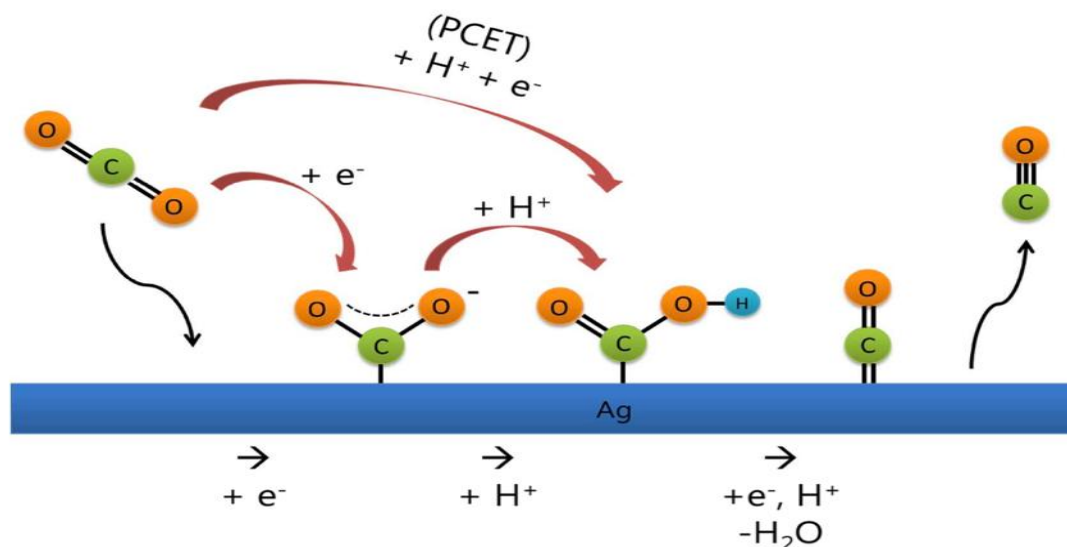
Figure 3 A schematic depiction of proposed CO_2 reduction to CO reaction mechanism on thin film Ag catalyst (28)

Hatsukade et al. exhibited the results from the potential dependent activity and selectivity on silver surfaces. The outstanding faradaic efficiency of CO among other products, however , the overpotential regions are also affect selectivity of main products (fig 4.) (26). This reflects the kinetics and mechanism of CO_2 reduction reaction. Ma et al. shown result from oxide-derived silver (OD-Ag) for CO_2 reduction to CO. The overall CO production faradaic efficiency of oxide-derived Ag was prominently displaced toward the positive potential compared to untreated Ag. The electroreduction of CO_2 to CO of the OD-Ag was 80% faradaic efficiency at -0.6 V vs. RHE. Moreover, OD-Ag can create a local pH around OD-Ag surface which promote activity with significantly suppressed HER (29).
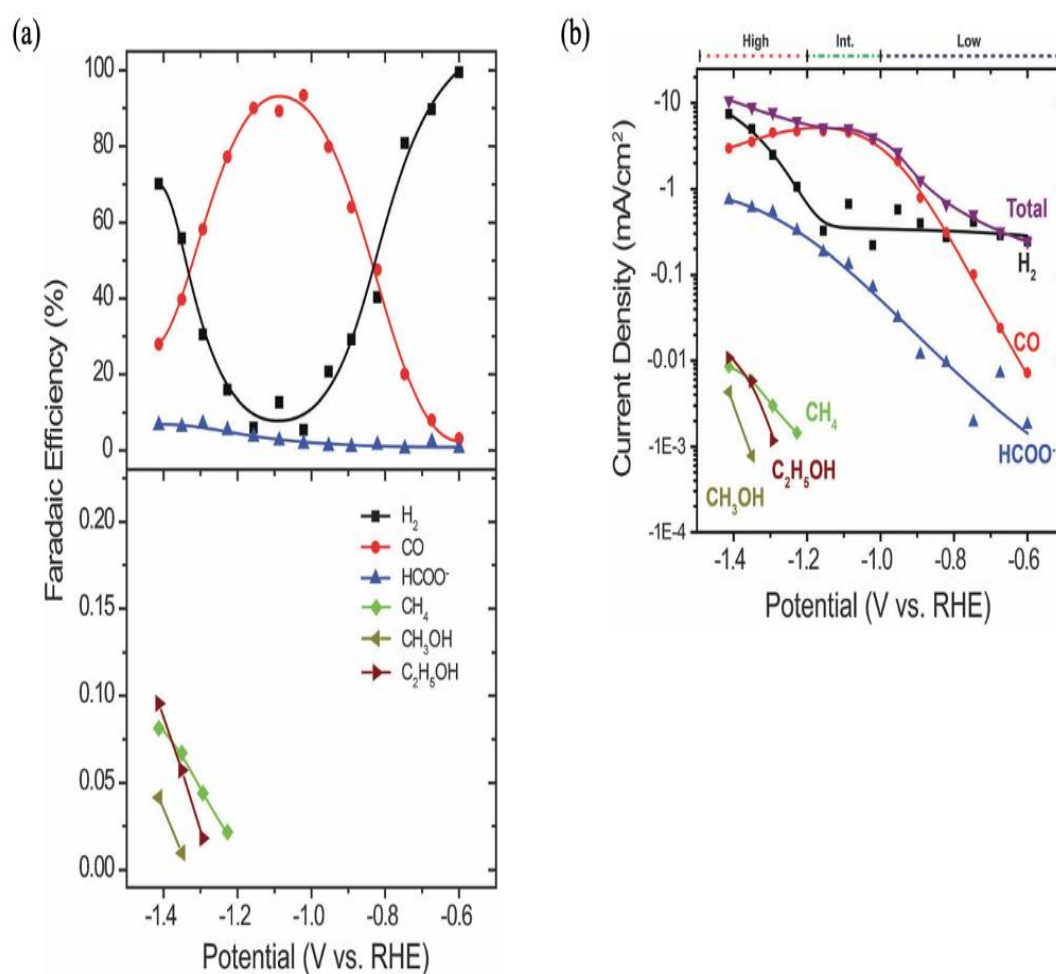
Figure 4 (a) Faradaic efficiency for each product as a function of potential, and (b) Tafel plot of the partial current density going to each product at different overpotential regions (26)

2.1.4.3 Zinc (Zn)

Zinc (Zn) is another metal which categorized as a CO or $HCOO^-$ forming metal. Luo W. et al. synthesizes porous Zn electrocatalyst using facial electrodeposition for CO_2 electroreduction to CO as shown in fig.5. The electrocatalyst can convert CO_2 to CO with 95% of faradaic efficiency and 27 mA cm$^-2$ at -0.95 V vs. RHE in 0.1 M $KHCO_3$ in H-type cell. While a flow cell reactor can reach 84% CO faradaic efficiency at -0.64 V and 200 mA cm^{-2} using Zn gas diffusion electrode (30).
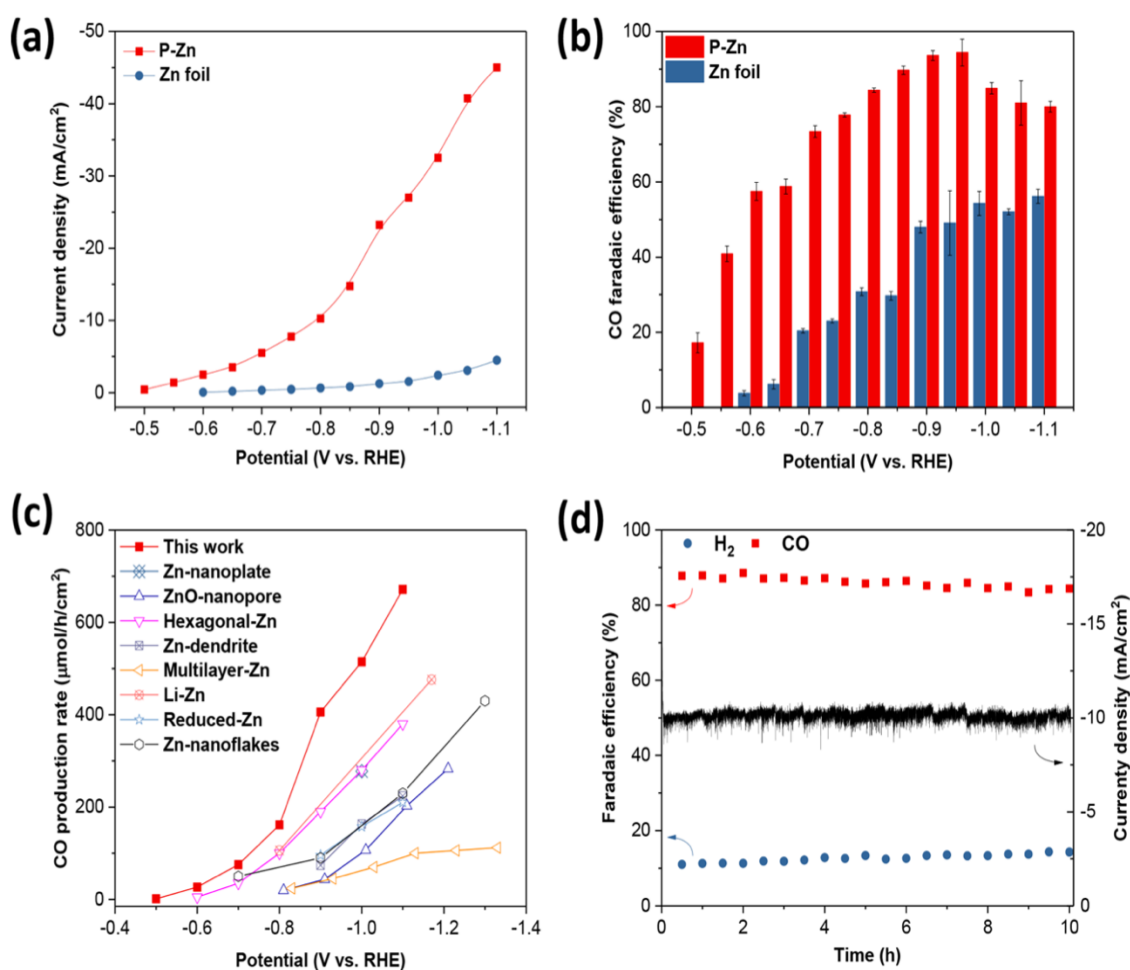
Figure 5 CO_2 reduction performance of P−Zn and Zn foil. Potential-dependent current density (a) and CO faradaic efficiency (b) for P−Zn and Zn foil. (c) Comparison of CO production rate observed over P−Zn and other state-of-the-art nanostructured Zn catalysts. (d) Catalytic stability for P−Zn (30)

Rosen et al. synthesized nanostructured Zn dendrite electrocatalyst using an electrodeposition method for CO_2 conversion under ambient conditions. The Zn dendrite catalyst activity and CO faradaic efficiency are obviously higher than that compared to the bulk Zn catalyst in an aqueous bicarbonate electrolyte as shown in fig.6 (31).
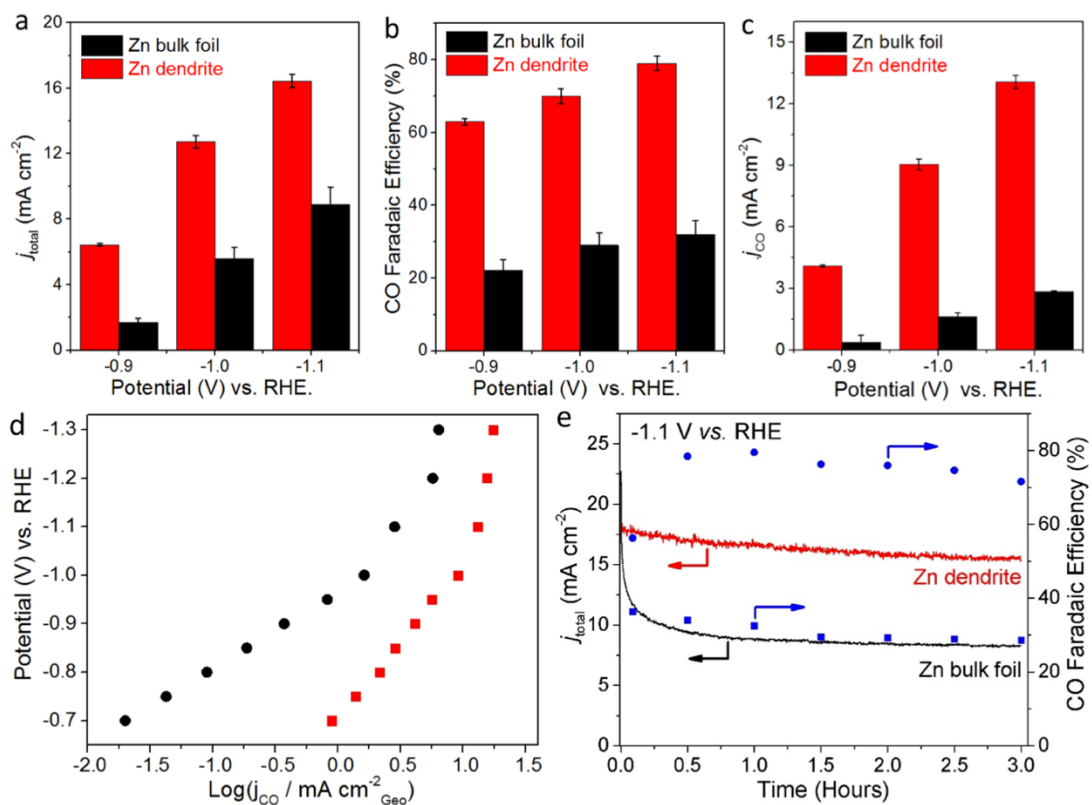
Figure 6 Comparison of (a) total current density, (b) CO faradaic efficiency, and (c) CO current density for bulk and dendritic Zn electrocatalysts. (d) Plot of log (jCO) vs. potential for Zn bulk foil (black) and Zn dendrite (e) Constant potential studies of bulk and dendritic Zn catalysts at - 1.1 V vs. RHE. The bulk symbols represent the CO faradaic efficiencies (31)

2.1.5 Electrolyte

Electrolyte plays important role in electrochemical reaction. The general properties should include good ionic conductivity, stable pH and absorption CO_2. Different type of electrolytes, concentration and pH affect to the product quality (32). The effect of pH in CO_2 reduction depends on electrolyte species (cation/anion) and its concentration. Bumroongsakulsawat et al. investigated the influence of pH on CO_2 reduction product selectivity in term of CO and $HCOO^-$ ratio at Sn electrode. A change in ratio from 1 to 0.15 in pH 2.9 (0.1 M H_3PO_4/1 M NaH_2PO_4) to pH 7.8 (9.5 M NaOH) was observed. According to the results, decreasing pH enhanced the partial current densities of CO and $HCOO^-$. Moreover, low pH was correlated with increasing in HER leading to decreasing in CO_2 reduction (33).
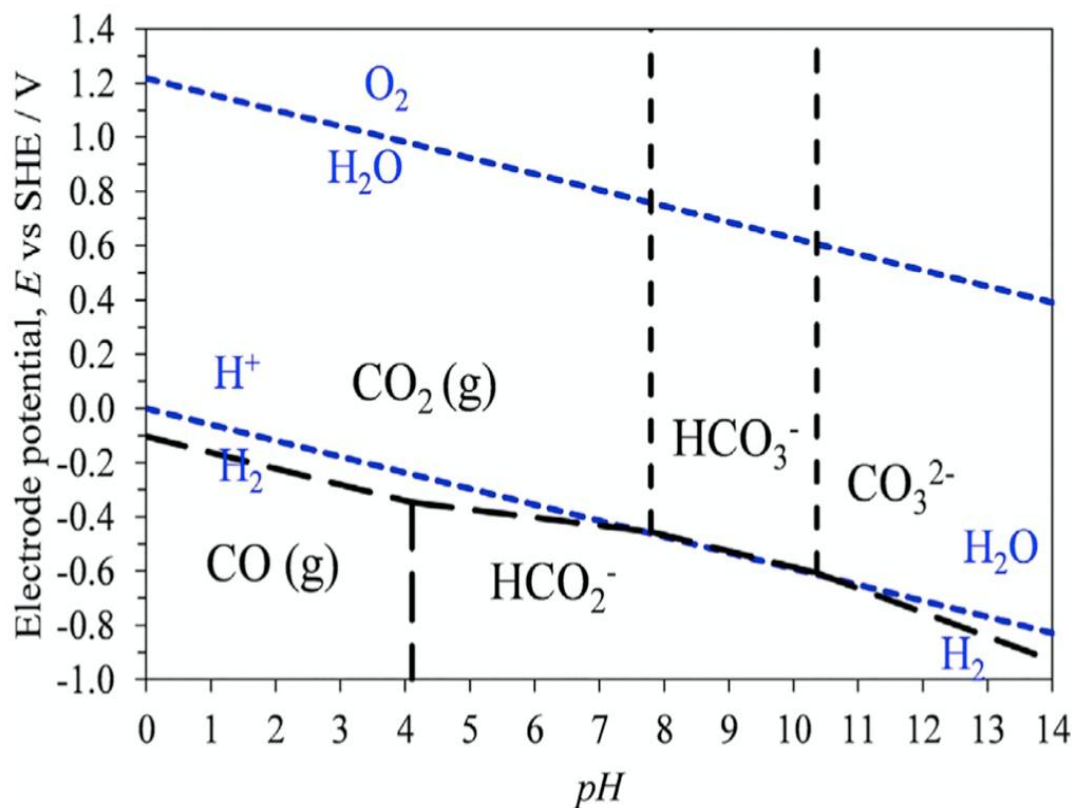
Figure 7 Meta-stable potential-pH diagram for C-H$_2$O system considering C^{IV}/C^{II} equilibria only at 298 K and 105 Pa. (33)

The selectivity and activity of CO$_2$ reduction relatively depend upon the local environment around the electrode such as pH value, CO$_2$ concentration, and electrolyte concentration. Nevertheless, the electrolyte is not the priority in the commercial process of CO$_2$ reduction as main targets regarding the performance. Yet, the separation and recycling of electrolyte still the issue to be manage, environment concern, and upscaling complexity.

2.1.6 Electrochemical cell for CO_2 reduction

The design of electrochemical cells is a critical step in CO_2 reduction, influencing cell performances such as current density, faradaic efficiency, and stability. Since Hori 's first revealed CO_2 reduction research in the 1980s, various cell designs have been investigation to improve CO_2 reduction reaction.

2.1.6.1 H-type cell

Fundamentally, H-type cell is lab-scale reactor for CO_2 Reduction, which widely used for gas and liquid products such as CO, and hydrocarbons. In this cell, both the working electrode and reference electrode are set in cathode chamber while the counter electrode is set in anode chamber. These electrodes are connected to external power supply and these two chambers are separated by ion-exchange membrane. Lu Q. et al. reported results from a nanoporous silver electrocatalyst in H-type cell. The CO selectivity approximately 92%. although this cell has feasibility on concept demonstration, but it still requires addition investigation for practical scale-up (34, 35).
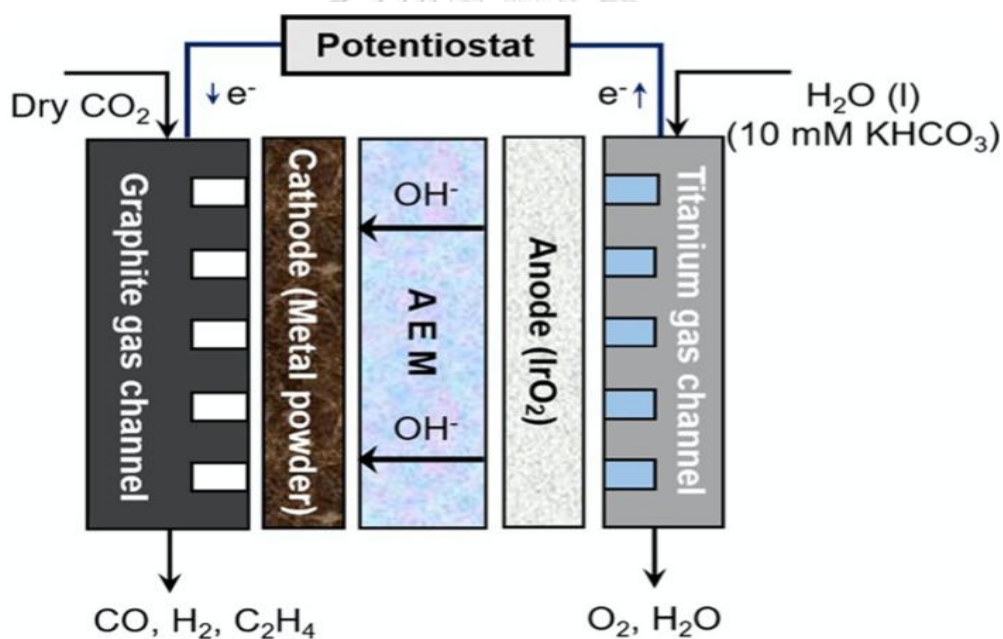
Figure 8 PEM Cell Scheme of an alkaline MEA cell for electrochemical CO_2 reduction. (35)

2.1.6.2 Polymer electrolyte membrane (PEM) flow cell

This type of flow cell has potential to surmount the limitations of H-cell and it is a more promising technology for scale-up applications Membrane electrode assembly (MEA) is deposition of catalysts on ion exchange membrane. PEM flow cells can be classified in three classes: cation-exchange membrane (CEM), anion exchange membrane (AEM) and bipolar membrane (BPM). A CEM has potential to transport cations from anode to cathode. in contrast an AEM facilitates anions from cathode to anode. A BPM consists of cation and anion exchange membrane that water is dissociated to OH^- and H^+, leading to constant pH, high current densities (36).

2.1.6.3 Microfluidic flow cell (MFC)

This electrolytic cell focuses on flowing of thin electrolyte channel between cathode and anode. The design of the flowing electrolyte is capable of tailoring operation conditions, including pH, and water management issues (37). Gabardo et al. reported a nearly 100% CO selectivity with the lowest overpotential 300mV at 300 mA cm^{-2} using an Ag-based GDE in microfluidic reactor as shown in fig.9. These improvements operated in a high alkaline condition and pressurized system (38).
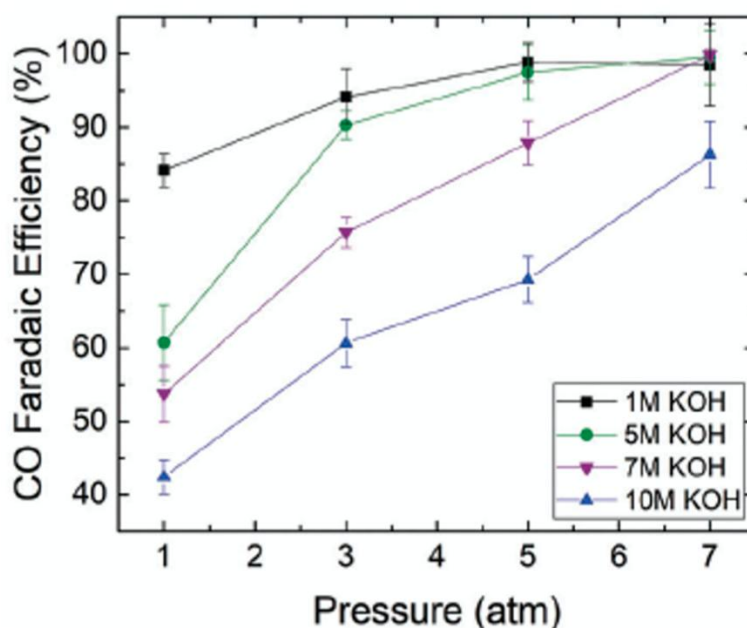
Figure 9 Effect of pressure on CO_2 reduction at 300 mA cm^{-2} at various pressures and KOH concentrations on CO faradaic efficiency. (38)

2.1.6.4 Solid-oxide electrolysis cell (SOEC)

For CO_2 reduction at high temperature, a solid oxide electrolysis cell (SOEC) has been attracting due to its high efficiencies. The advantage of high temperature is promoting kinetics of reaction and reduces internal resistance Ye et al. have shown high performance CO_2 electrolysis with ca. 100% faradaic efficiency. The doped strontium titanate cooperated with Ni particle enables high temperature adsorption, activation and thermal stability with non-degradation after 10 redox cycles for 100 h (39). CO_2 electrolysis using a Ni/YSZ electrode supported solid oxide electrolysis cells (SOECs) was reported by Ebbesen et al. The passivation rate of the SOEC range was 0.22 to 0.44 mV h^{-1} when reaction took place at current densities between -0.25 and -0.50 A cm^{-2} in ratios of CO_2/CO = 70/30 or CO_2/CO = 98/02 at high temperature (40). However, SOEC has drawbacks due to its temperature operation, including carbon deposition, metal oxidation and cell degradation.
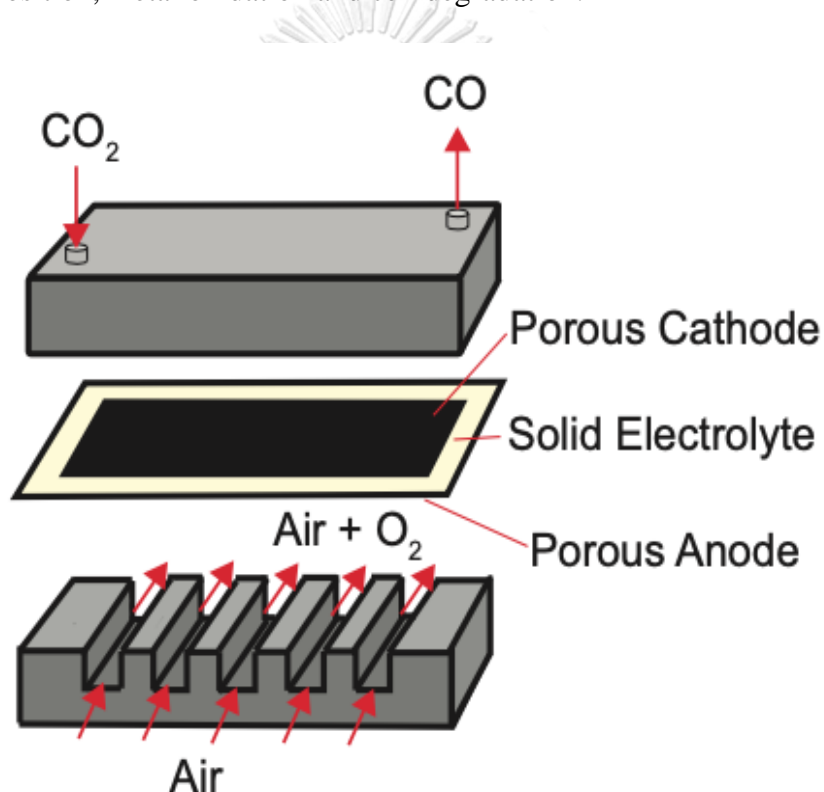
Figure 10 A Schematic diagram of solid-oxide electrolysis cell. (41)

2.2 Literature reviews

The complication of the CO_2RR pathway is difficult to achieve the CO product efficiently. Hence, it is significant to develop productive catalyst and technology for CO_2RR. Hori and co-worker convert CO_2 in 0.2 M K_2SO_4 solution using silver-coated ion exchange membrane electrodes (solid polymer electrolyte: SPE). The effect of membrane types (CEM and AEM) and SPE preparation were investigated. The Ag-coated SPE/AEM electrode CO_2 reduction result is remarkably over SPE/CEM electrode. They also compared the ultrasonic radiation and unmodified SPE/AEM. The ultrasonic electrode enhanced current density to 92% current efficiency at 20 mA cm^{-2}, in contrast, unmodified SPE reaches 74.4% current efficiency. The partial CO_2 current density is 60 mA cm^{-2} that three times higher than upper limit of conventional electrode obtained compared to Ag electrode (42).
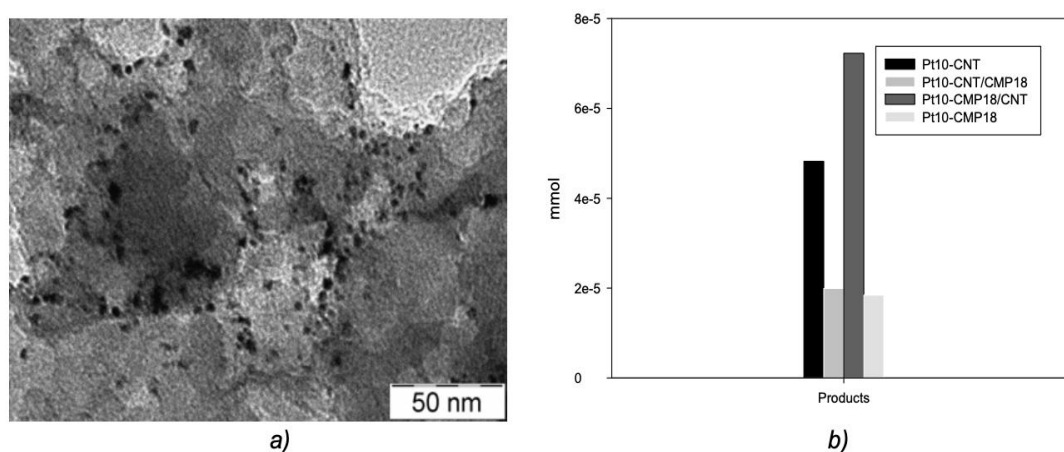
Figure 11 a) TEM image of Pt nanoparticles on the TPE-CMP surface; b) productivity for Pt doped CNT and TPE-CMP electrocatalysts (amount of metal: 10 wt. %, current: -20mA, T=60°C). (43)

As mentioned in early section, the utilisation of CO_2 in an aqueous solution brings mass transfer limitations that hinder scale-up. The continuous flow reactors: membrane reactor, micro-reactor, packed-bed reactor was developed configuration and design to maximise surface-to volume ratio. Electrocatalysts designed by Ampelli et al. for gas phase CO_2 reduction consist of conjugated microporous polymers (TPE-CMP) doped with Pt nanoparticles as shown in fig.11 and mixed with carbon nanotubes (CNT). The results indicated that an assembly of Pt metal, CMP and CNT is the key to improve proton mobility and electron conductivity. The electrocatalysts exhibited a good performance in terms of C1-C3 liquid product formation with at least 95% faradic efficiency (43). Jingjie Wu et al. converted CO_2 to formate in microstructure electrochemical cell as shown in fig.12 operated at a low current density (<30 mA cm^{-2}). The results in fig.13 were reported in term of nafion loading, catalyst thickness layer and catalyst size particle. The Sn catalyst average particle size of 100 nm to 1.5 micrometer with 17-20 wt.%Nafion was found the highest in both current density and faradaic efficiency at -1.6V vs SCE. The effective catalyst thickness is 9 nm at -1.6V vs SCE with 20 wt.%Nafion and 100 nm of Sn (44).
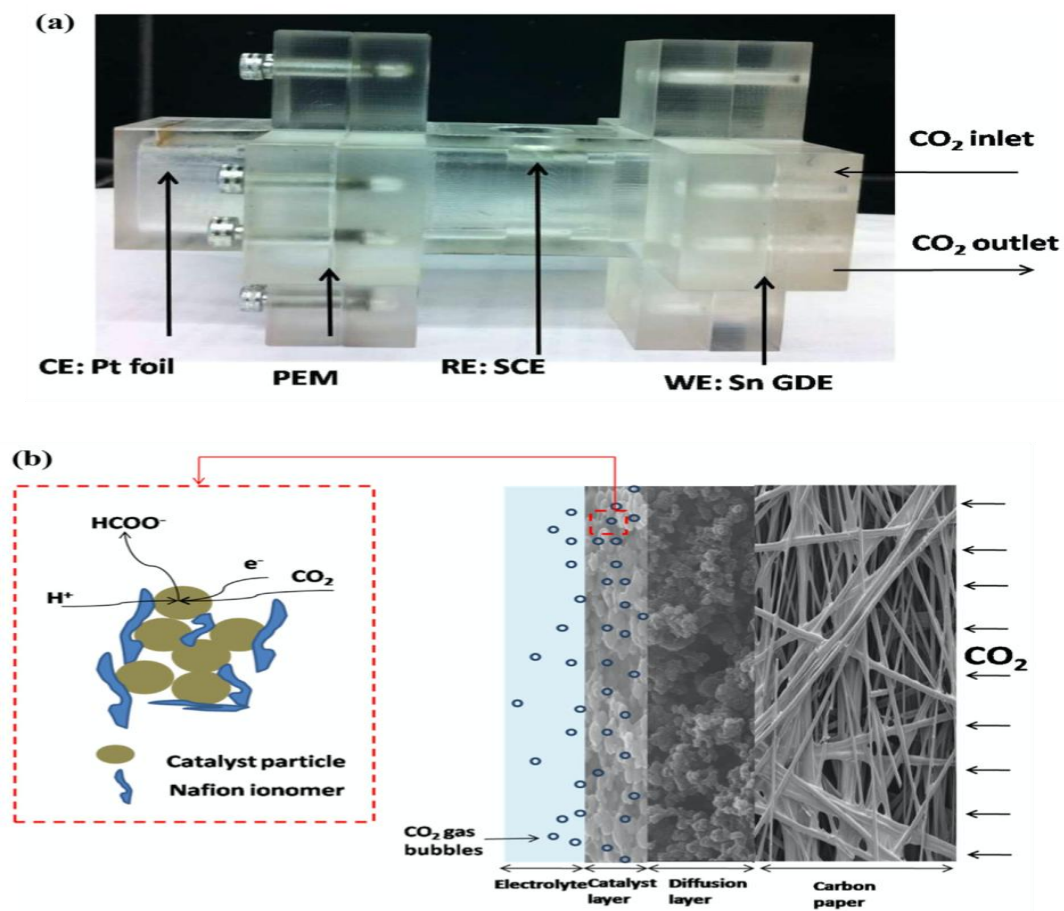
Figure 12 (a) A cell setup for measuring the electrocatalytic activity of Sn GDEs towards CO₂ reduction and (b) schematic of CO₂ reduction at the triple-phase interfaces. (44)
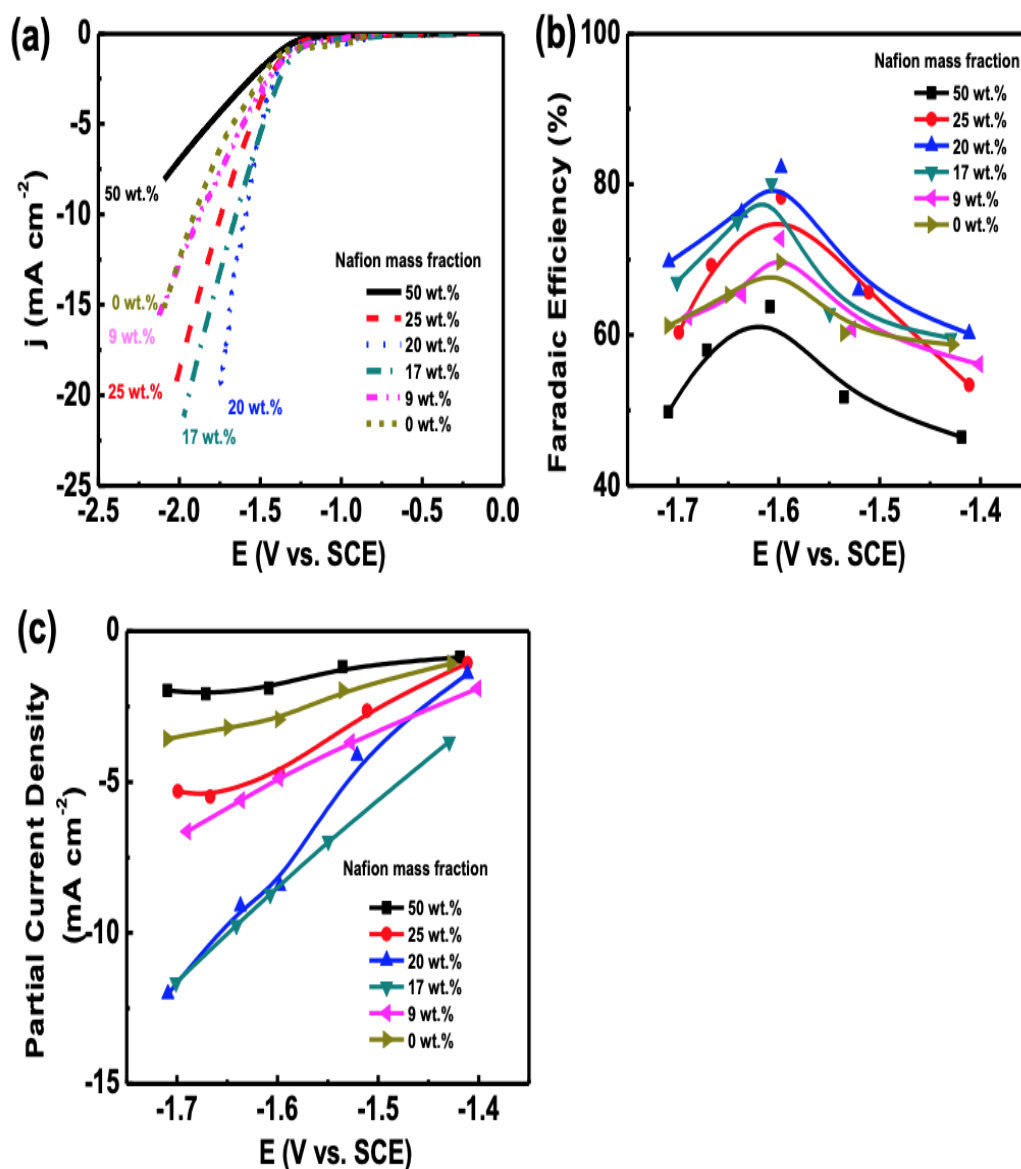
Figure 13 (a) ieV curves of three independent Sn GDEs for CO_2 reduction before iR compensation, (b) EIS measurement of ohmic resistance, (c) iV curves after iR compensation. The inset in (b) is a magnification of impedance in high frequency. (44)

The highly selective nickel nitride (Ni_3N) electrocatalyst was used for reducing CO_2 in both the aqueous phase and the gas phase compared to Ni and NiO that generated H_2. Hou reported 85.7% of CO faradaic efficiency was observed in aqueous solution with partial current density 6.3 mA cm^{-2} at -0.90 V vs. RHE. When CO_2 flew through using the membrane-electrode assembly (MEA) consisted on anion-exchange membrane, current density reached 23.3 mA cm^{-2} with the CO faradaic efficiency raised to 92.5% (45).
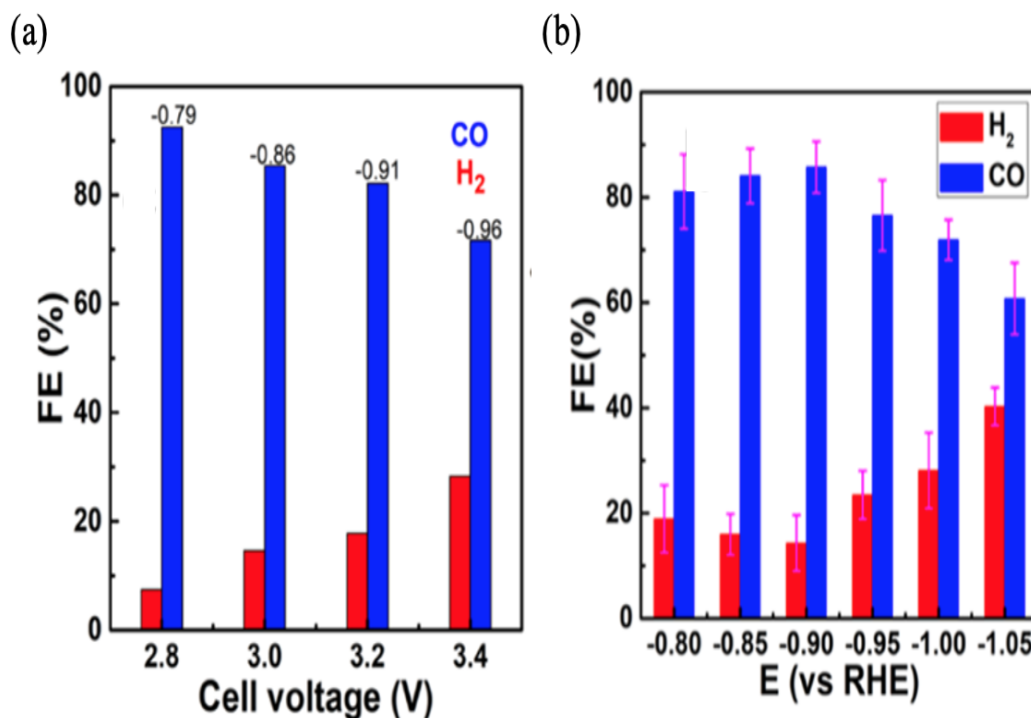
Figure 14 Gas electrolysis in a flow cell. (a) FEs for CO (blue) and H_2 with different cathode potential vs NHE, (b) FEs for CO (blue), and H_2 with Ni_3N/C. FEs for CO and H_2 with Ni/C. (45)

Gas diffusion electrodes (GDE), solid polymer electrolyte (SPE),and ion exchange membranes, where the catalysts are deposited directly on the membranes, are wildly used for electrochemical CO_2 reduction. Wang et al. reported conversion of humidified CO_2 to CO on proton-exchange and alkaline anion-exchange membrane as shown in fig.15 using conventional Pt/C, Pd/C and Cu/CNTs as cathodic catalyst. Figure 16 shown a result form AAEM was successful in converting CO_2 to CO while PEM has no activity for CO_2 reduction. AAEM reactor also facilitates the CO_2 reduction reaction and prohibits the hydrogen evolution reaction (HER) at the cathode. Cu/CNT cathode catalysts shows a higher activity to convert CO_2 to CO among the other catalysts at the same catalyst loading (46). Kim studied the effect of dilute feed and pH on electrochemical reduction of CO_2 to CO in flow cell using Ag-GDE. The results confirmed even dilute CO_2 (10%) could be reached more 80% CO faradaic efficiency with 29 mA cm^{-2} of CO current density at 3.0 V though current density is 55% less when operating with 100% CO_2 feed (47).
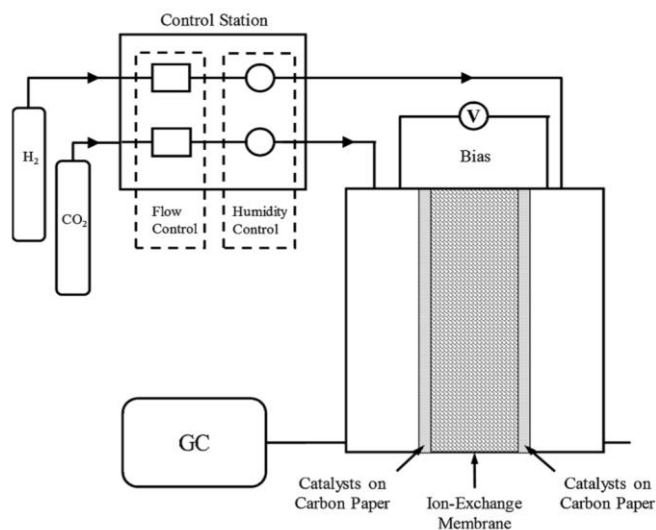
Figure 15 The setup for the gas phase electrochemical conversion of CO_2 in a fuel cell reactor. (46)
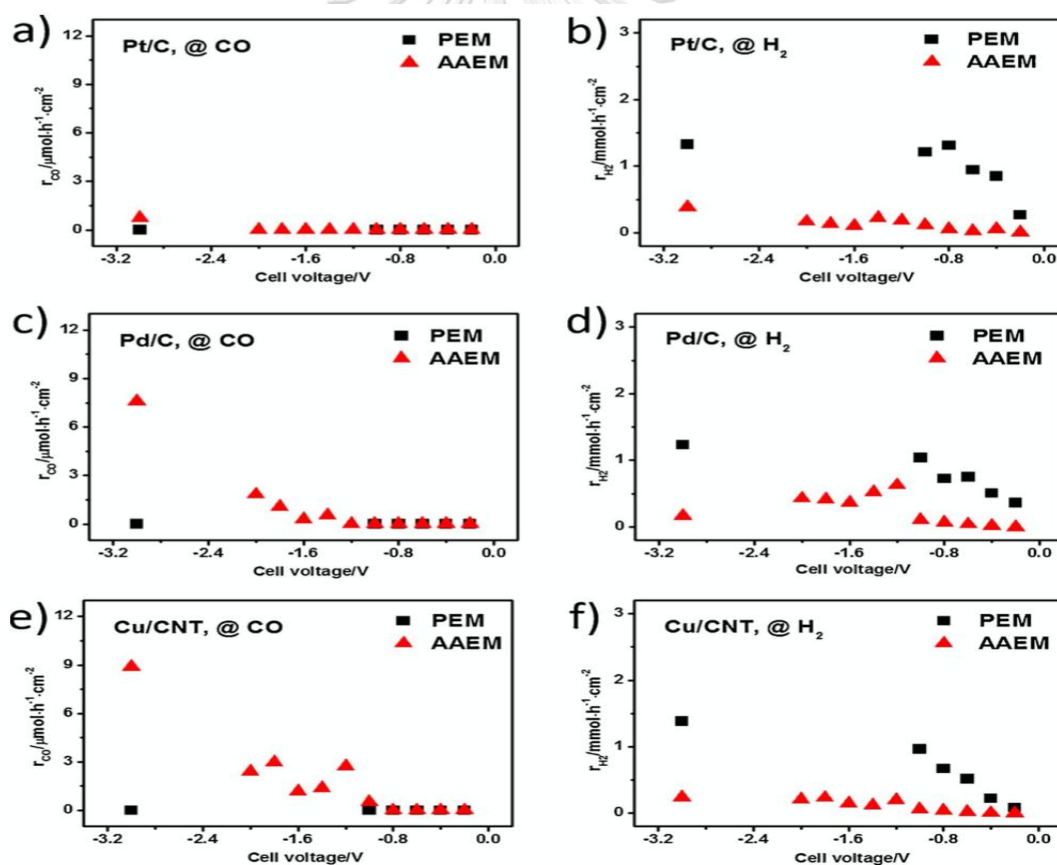
Figure 16 Production rates of gas products of CO_2 conversion on PEM and AAEM based fuel cell reactors with different cathode catalysts at 40 °C: (a,b) Pt/C, (c,d) Pd/C, and (e,f) Cu/CNTs. (46)

Yang et al. developed a novel three-compartment reactor for CO_2 reducing to formic acid. The reactor consists of a cation-exchange membrane and anion-exchange membrane. The cell produced formic acid operated at a current density of 140 mA cm^{-2} with formic acid faradaic efficiencies of up to 94% at a cell voltage of 3.5 V (48).
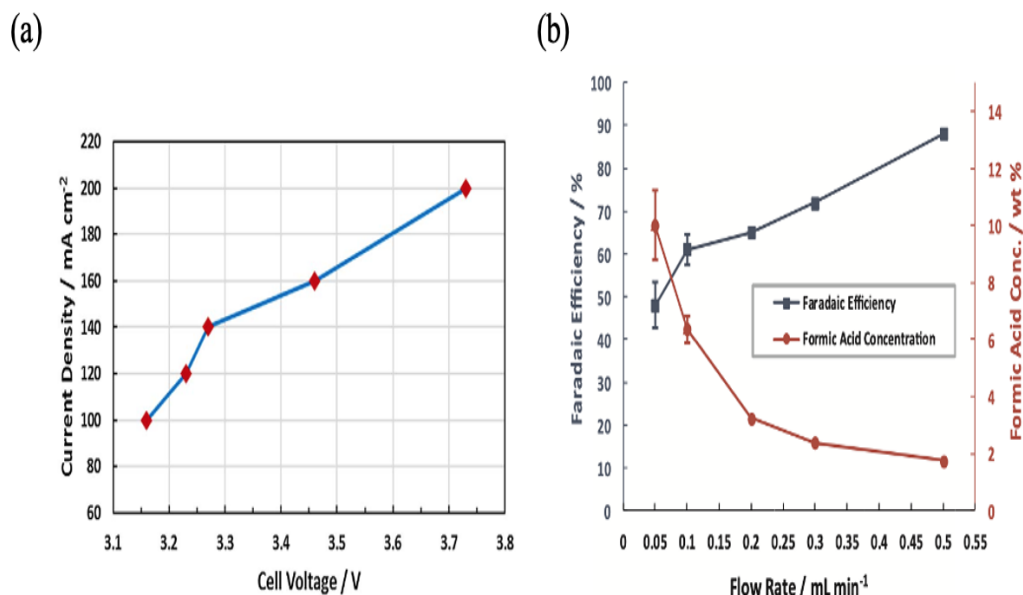
Figure 17 The results from typical cell configuration in a single pass operation (a) current density, (b) Faradaic efficiency of formic acid. (48)

Delacourt and co-workers design electrochemical cell synthesis syngas from CO_2 and H_2O at ambient conditions. The effect of Ag GDE catalysts with and without a pH buffer layer ($KHCO_3$ aqueous solution) was studied. The results show that the pH buffer layer cooperated with the CEM system enhance CO selectivity to 80% and prohibited HER at -1.7 to -1.75 V vs SCE. While CEM configuration (fig.18a) suppressed CO_2 reduction reaction, leading to HER only. This pH buffer layer prevents excess amount of H^+. Nevertheless, the presence of buffer layer in a modified CEM is not a suitable design for realistic application. To simplify a modified CEM, AEM configuration (fig.18c) was developed and obviously improved efficient of CO_2 reduction compared to CEM (49).
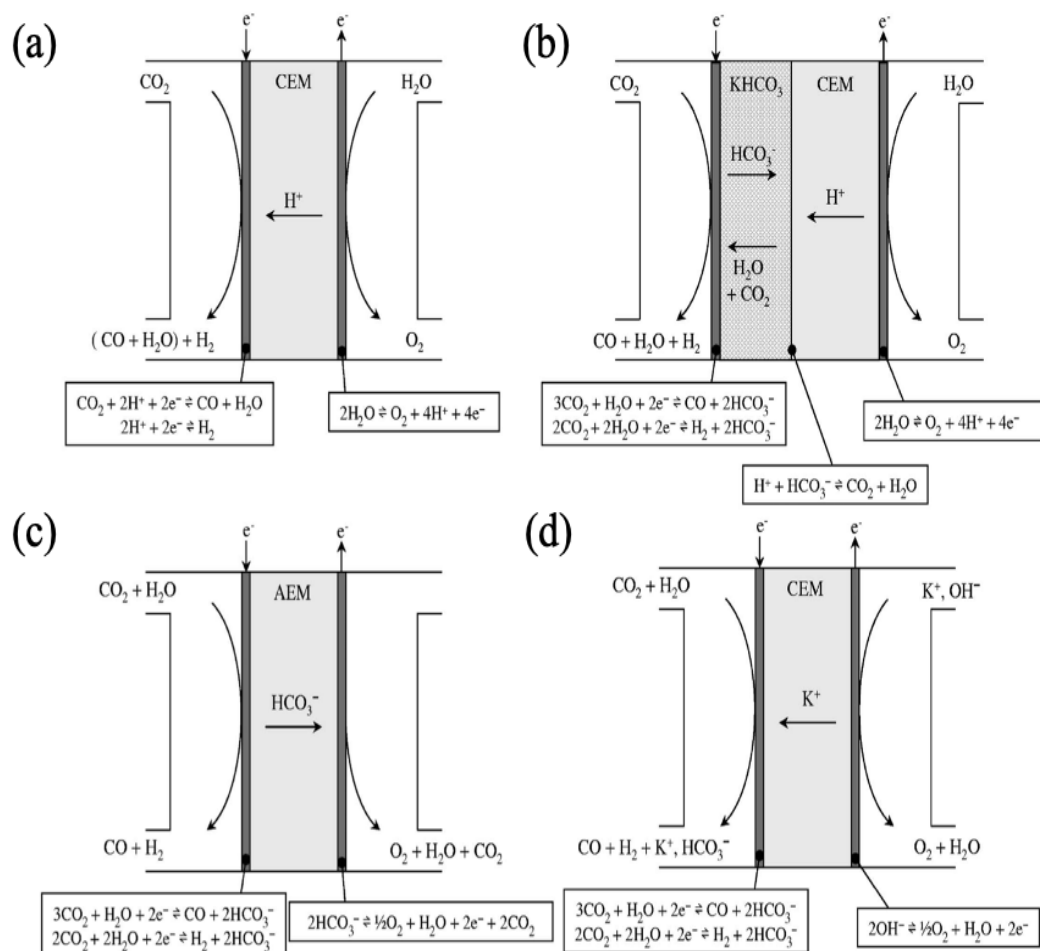
Figure 18 (a) Electrochemical cell with a cation-exchange membrane (CEM). (b) Modified electrochemical cell with a pH-buffer layer and the CEM. (c) Electrochemical cell with an anion exchange membrane (AEM). (d) Electrochemical cell based on a CEM in the K^+-form. (49)

Verma et al. used a supported gold catalyst on polymer wrapped carbon nanotubes in an alkaline electrolyzer which provides high conductivity and high activate surface area. The electrolyzer exhibits high j_{CO} and overpotential at -0.55 V vs. RHE. The tefal slopes as shown in fig 19 indicates the rate limiting step for the CO_2 to CO is a pH independent. Thus, increasing pH of system can obtain high cell overpotentials (50). Dufek shown results from a pressurized electro-chemical cell for continuous CO_2 reduction at high pressure, using an Ag-based cathode. The quantity of produced CO at elevated pressure is 5 times higher than ambient pressure with 92% faradic efficiencies observed at 350 mA cm^{-2}. Their research also demonstrates benefits of increased temperature. At 225 mA cm^{-2} and 18.5 atm, Increased temperature from 60 to 90°C contributed to a cell voltage below 3V as shown in fig.19 equal to an electrical efficiency of 50%. (51).
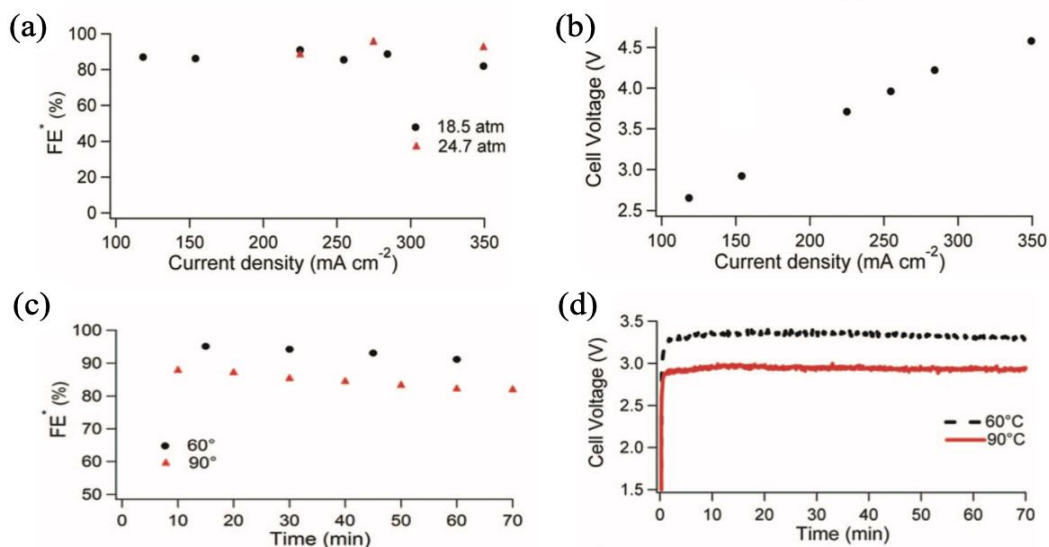
Figure 19 Comparison of cell performance at 60 and 90°C (0.5 M K_2SO_4 and 1.0 M $KHCO_3$ catholyte), CO_2 flow rate 150 mL min^{-1} at a–b) 18.5 atm and 225 mA cm^{-2}, c–d) 24.6 atm and 275 mA cm^{-2}. (51)

Dufek shown results from a pressurized electro-chemical cell for continuous CO_2 reduction at high pressure, using an Ag-based cathode. The quantity of produced CO at elevated pressure is 5 times higher than ambient pressure with 92% faradic efficiencies observed at 350 mA cm^{-2}. Their research also demonstrates benefits of increased temperature. At 225 mA cm^{-2} and 18.5 atm, Increased temperature from 60 to 90°C contributed to a cell voltage below 3V as shown in fig.19 equal to an electrical efficiency of 50% (52, 53).
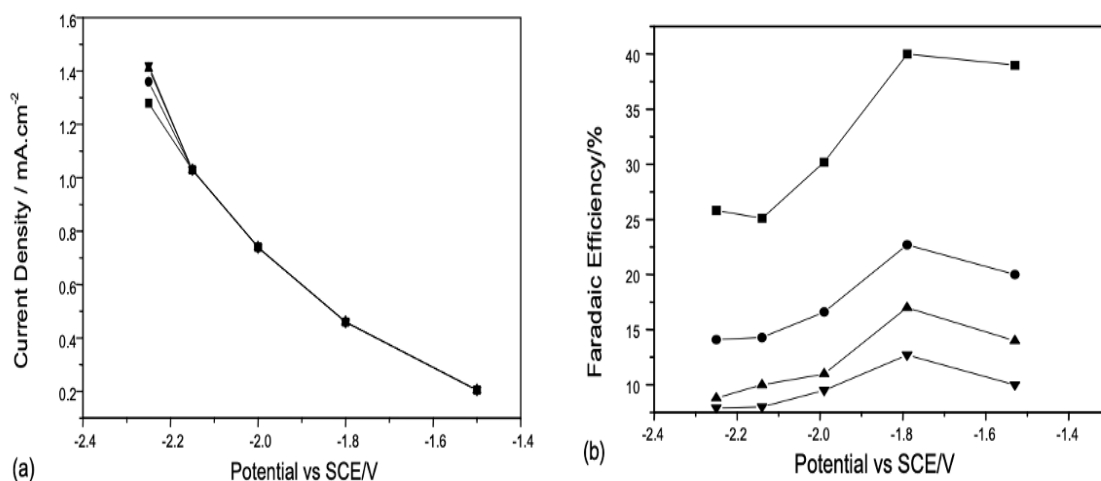
Figure 20 (a) The current density of CO_2 reduction on Pb electrode at various time periods. (b) Faradaic current efficiency for formic acid formation on Pb electrode at different time intervals. (52)

Monroe et al. introduced a one-pass lamilar flow cell in fig.21 for electrochemical reduction of CO_2 to liquid fuel products. To be practical, a laminar flow in the separation strategy is significantly require partitioning the formate-containing electrolyte (0.1 M $KHCO_3$) produced and prevent oxidation products at Sn cathode surface at 5 mA cm^{-2}. The product trends of the experimental separation efficiency with channel width (W) and flow rates were corresponding to model predictions but the separation efficiency values are generally lower than model. (54)
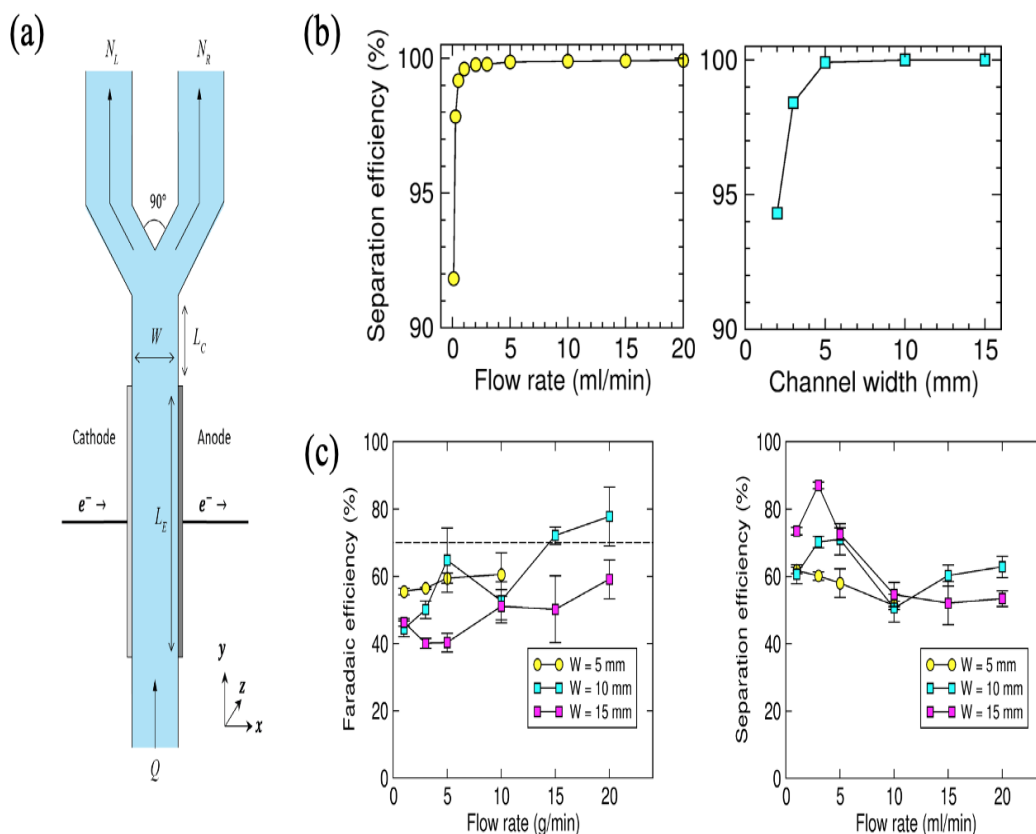
Figure 21 (a) Cross section view of the Y-channel geometry of the laminar CO_2 reduction flow cell. CO_2 reduction flow separation efficiencies as a function of physical variables. (b) Flow rate varied at fixed W = 5 mm and channel width varied at Q = 5 ml min^{-1}. (c) Overall faradaic efficiency and separation efficiency for formate production in laminar flow reactor. (54)

Hani reported the difference between a batch electrochemical cell and a flow cell for the electrochemical reduction of CO_2 using a porous gold cathode (55). The faradaic efficiency of CO in flow cell was 80-90% at any concentration, whereas in batch cell, the value dropped from 75% to 35% as the concentration is increased from 0.05 to 0.5 mol L^{-1}.
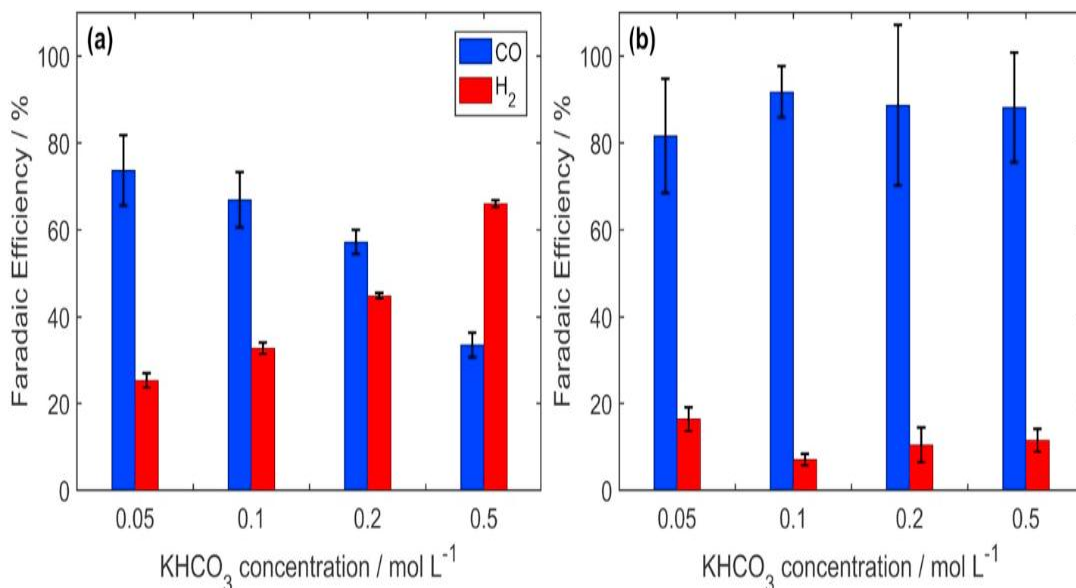
Figure 22 Faradaic efficiency for CO and H_2 (a) the batch cell; (b) the flow cell. (55)
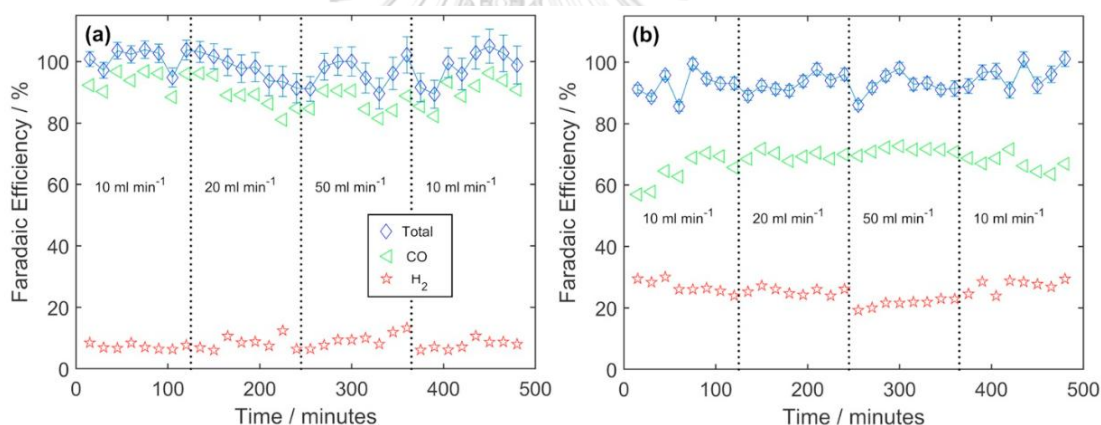
Figure 23 Faradaic efficiency changes in the flow cell by time at: (a) −1.3 V; (b) −1.5 V using 0.2 mol L^{-1} $KHCO_3$ as the catholyte and a CO_2 bubbling flow rate of 20 mL min^{-1}. (55)

To be more similarly required industrial conditions, Dufek (56) investigated on the effect of the elevated temperature on CO_2 electrochemical reduction. Increasing the temperature above room temperature increased CO EF as shown in fig.24 to a maximum at 35°C but then deceases at 70°C. This indicated the decreasing in CO_2 solubility with temperature. For cell performance, at 70°C and 70 mA cm^{-2} E_{cell} drops by 1.57 V from18°C to 70°C. The similar trend was observed in E_c decreased from -21.9 to -1.87 V for the same temperature. This indicates increasing in temperature minimize the process potentials needed. In case of effect of catholyte concentration and CO_2 flow rate toward syn-gas products (H_2:CO). The decreasing the CO_2 flow rate decreases amount of syn-gas produced as shown in fig.25.
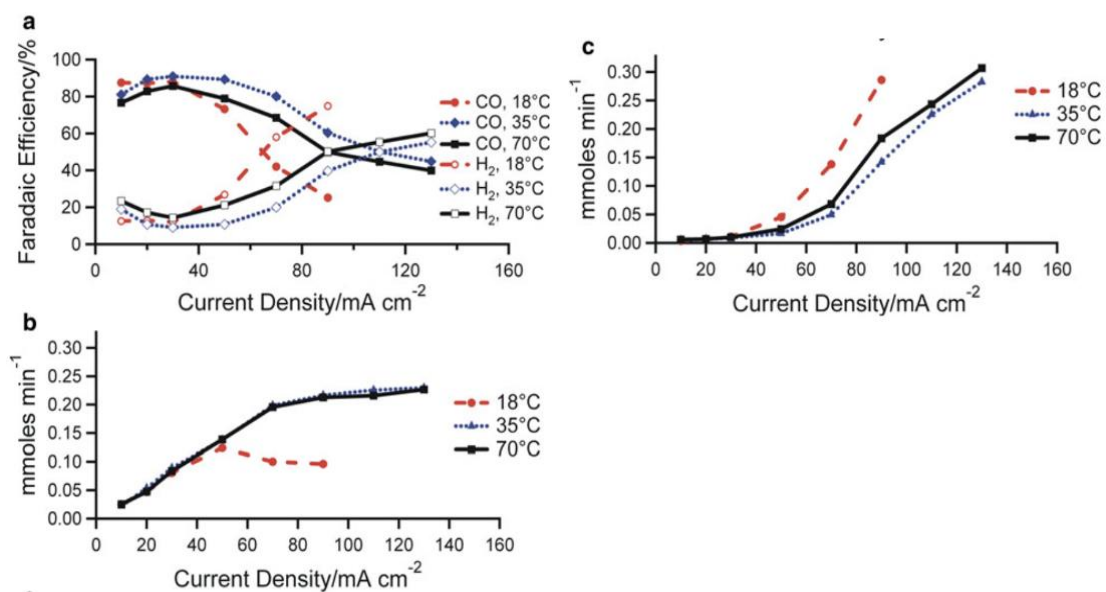
Figure 24 Cell performance at 18, 35, and 70 °C, CO_2 flow 20 mL min^{-1} (a) FE for CO and H_2 (b) rate of produced CO, and (c) rate of produced H_2. (56)
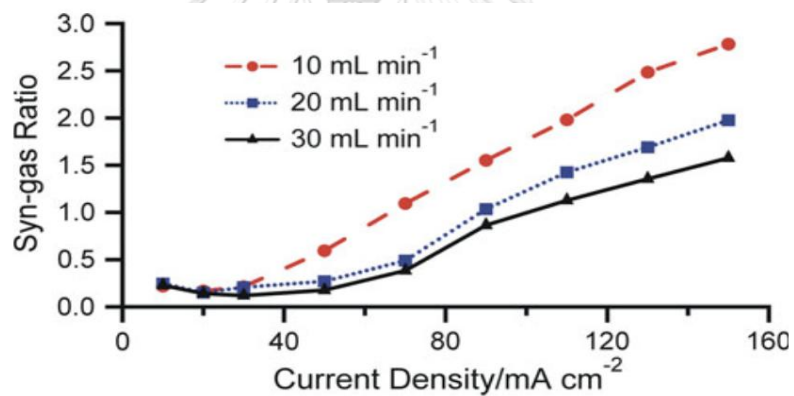
Figure 25 Syn-gas (H_2:CO) ratio as a function of CO_2 flow rate. (56)

Chapter 3
Methodology

3.1 Electrochemical cell

To achieve practical parameters for the electroreduction of CO_2, our cell design has been made to minimize complexity of cell components assembly. The novel electrochemical packed-bed reactor for CO_2 reduction in the gas phase is made from glass vessel that is shown in fig.26. The cell inside and outside diameter is 15 mm and 30 mm respectively with 6 mm of gas inlet. Titanium plates of 30 mm diameter are placed on the two ends to close to the cell chamber and are connected to a DC power supply. At the middle, electrocatalysts consisted of Zn-deposited felt, ion-exchange resin, and platinized titanium arranged in this order and fixed by the titanium mesh (Fuel Cell Store) connected with gold wire through the cell. EDPM (Fuel Cell Store) gaskets are inserted between the flange of the cell. C-clamps are used for holding the cell together. The cell was installed along the length of the reactor so that a gas stream could perpendicularly flow through all cell components.
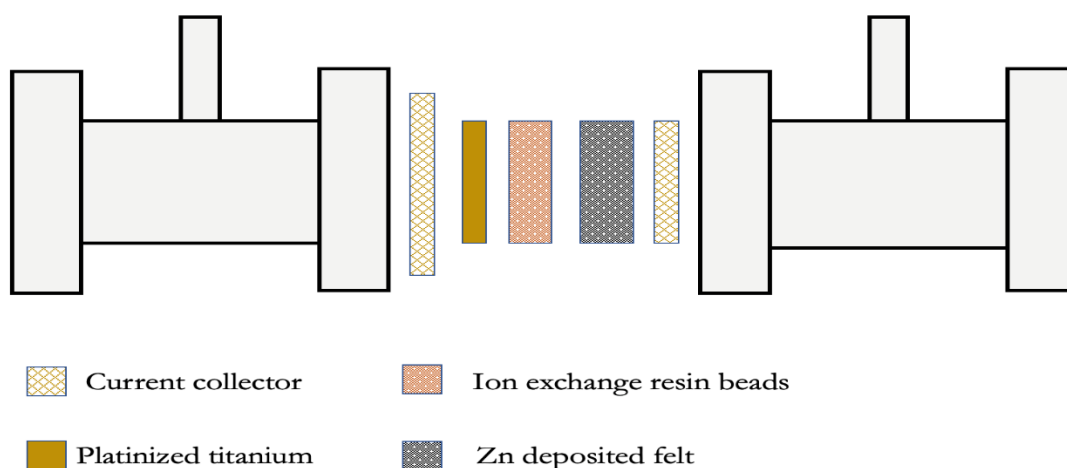
Figure 26 The novel packed bed electrochemical reactor compartments.

3.2 Preparation of Zinc deposition

Zinc was deposited on carbon felt (Fuel cell store) with size about 1.76 cm^2 at 30 mA in aqueous solution of 1 M $ZnSO_4$ at pH4 adjusted by 1 M H_2SO_4 for 2 hours. The Titanium plate (Local supplier) and platinized titanium mesh (Fuel cell store) with a dimension of 2*5 cm^2 were used as support of carbon felt. Before deposition, carbon felt was pressed to remove air inside the pore. The Zn deposited carbon felt was rinsed with deionized water then drying at room temperature. The morphology of Zn plated carbon felt was characterized by Scanning electron microscopy (SEM).

3.3 Procedure

The 0.5 g of ion exchange resin (Dowex Marathon MSA chloride form, Sigma-Aldrich) was immersed into an aqueous solution of 1 M NaOH for 30 min then rinsed with DI water before packed into the electrolytic cell. The Zn plated carbon felt was used as cathode. CO_2 (Linde, 99.995 %) was continuously fed through a saturator before it was passed to the cathode side at flow rate of 40, 80, and 120 mL min^{-1} controlled by a mass flow controller (MFC). The cell was always fed with CO_2 without applied voltage for 30 min to saturate the resin. For the experiments investigating the effect of the voltage, the voltage was adjusted from 3 (onset) to 6 V for 30 minutes. The voltage was then stopped for 5 min before starting the next batch to purge remaining gas products in the cell. An analogous set up was applied to a two-cell bed reactor with varying voltage between 8 to 11 V. CO concentrations were determined by an online IR spectrometer (Yokogawa, IR200-JNGHFGHKNN-4TU).
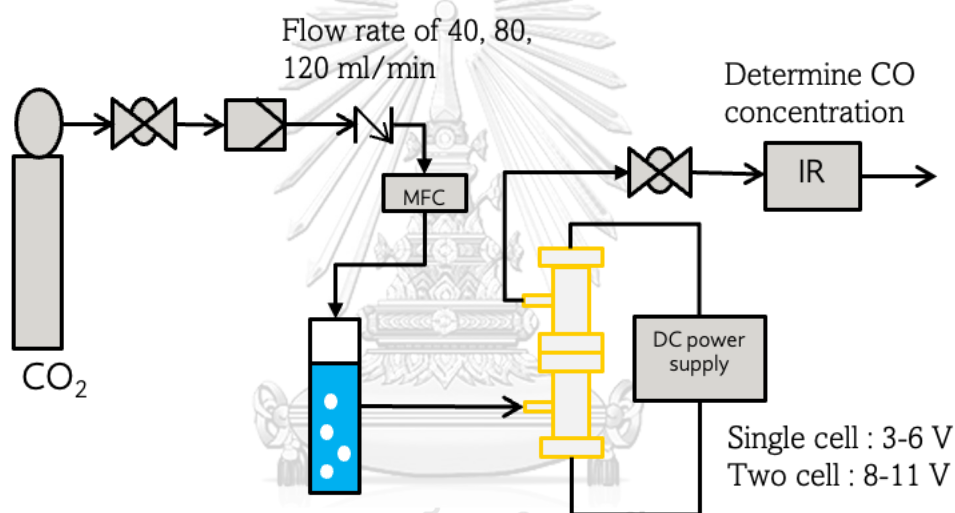
Figure 27 Process flow diagram of CO_2 reduction.

Chapter 4
Results and Discussion

The purpose of this work was to develop a novel electrochemical cell which could be scaled up. The applied voltage and flow rate were a focus because these parameters were required for industrial operation. Figure 28 shows a SEM image of zinc-carbon felt followed by the method described in Section 3.2. The zinc particles deposits appeared to cover the carbon fiber.
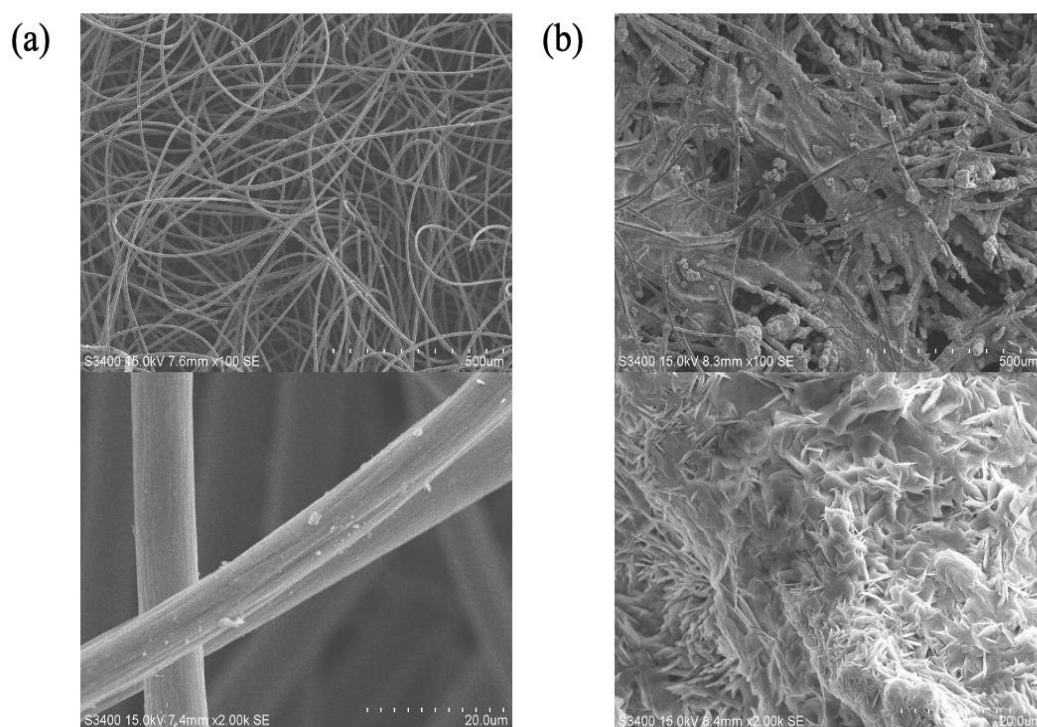
Figure 28 SEM analysis of (a) Carbon felt, and (b) Zn deposited carbon felt.

4.1 CO$_2$ reduction

4.1.1 Single-cell bed reactor.

Figure 29, 30 and 31 show the effect of applied potentials toward the electrochemical CO$_2$ reduction with Zn deposited felt. For single-cell bed reactor, the CO concentration was started forming at 4 V at any CO$_2$ flow rate. This evidence indicates that the minimum voltage for driving the reaction need at least 4 V for single-cell bed reactor. The current and CO concentration were corresponded with increased applied voltage. The CO concentration increased from 828 ppm for 40 ml min^{-1} to 1825 ppm for 80 ml min^{-1} at 6 V which increased CO Faradaic efficiency from 1.72% to 14.66%.
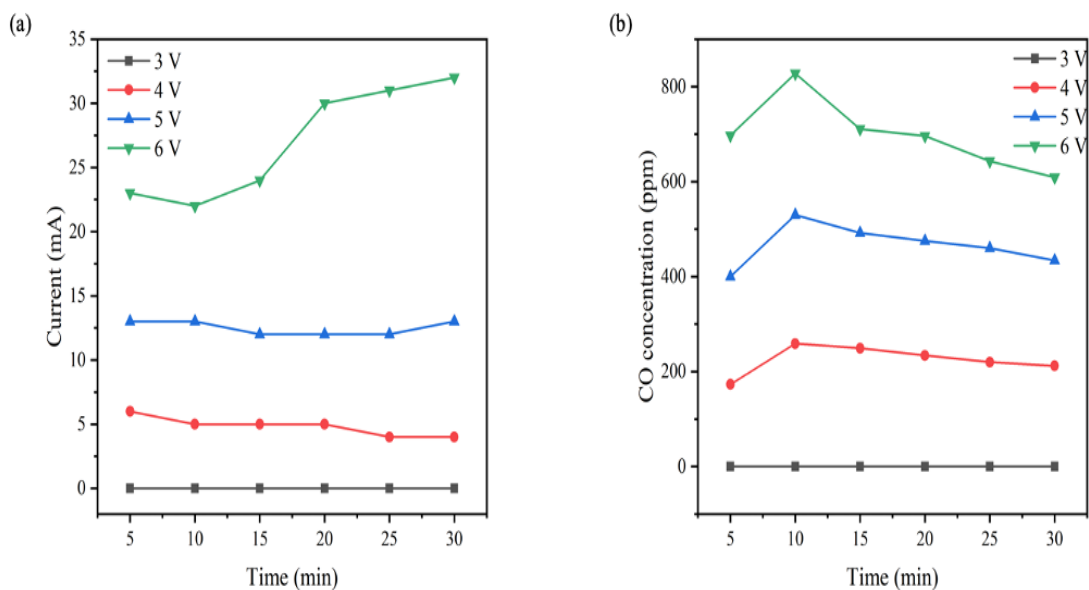
Figure 29 CO concentration (ppm) and current (mA) for CO_2 flow rate of 40 ml min^{-1}.

The plateau of current of ~ 5mA and ~15 ma at 4 and 5 V respectively for all flow rates implies that the reaction becomes mass transfer limited under these conditions. Although the limiting current plateaus presents at flow rate of 80 and, 120 ml min^{-1}, the CO concentration monotonically escalate under applied voltages of 5 and 6 V. These results might be a consequence of a high flow rate indicated that the CO concentration partially depends upon mass transfer of CO_2 to the felt surface.
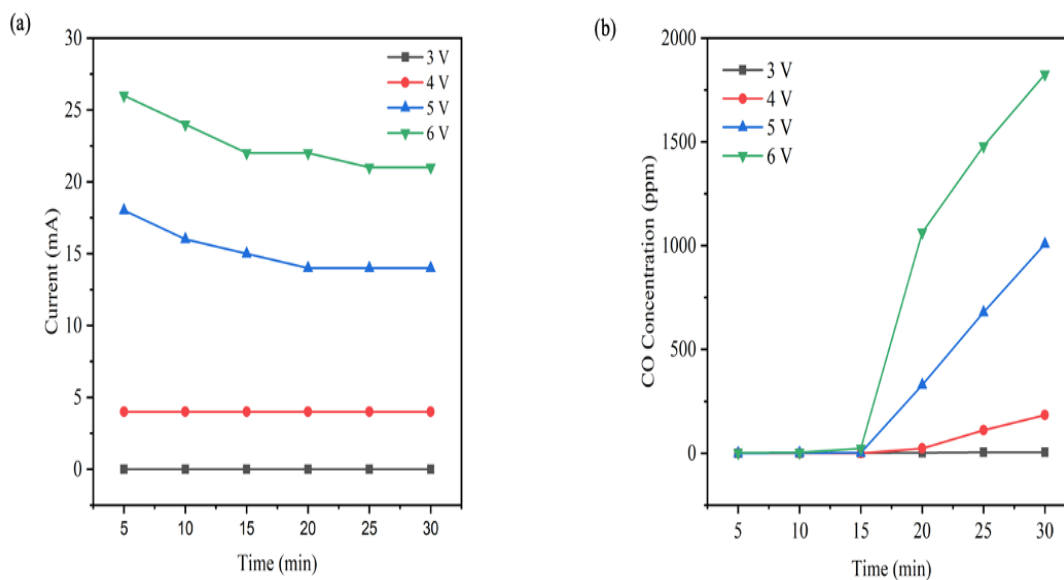
Figure 30 CO concentration (ppm) and current (mA) for CO_2 flow rate of 80 ml min^{-1}.
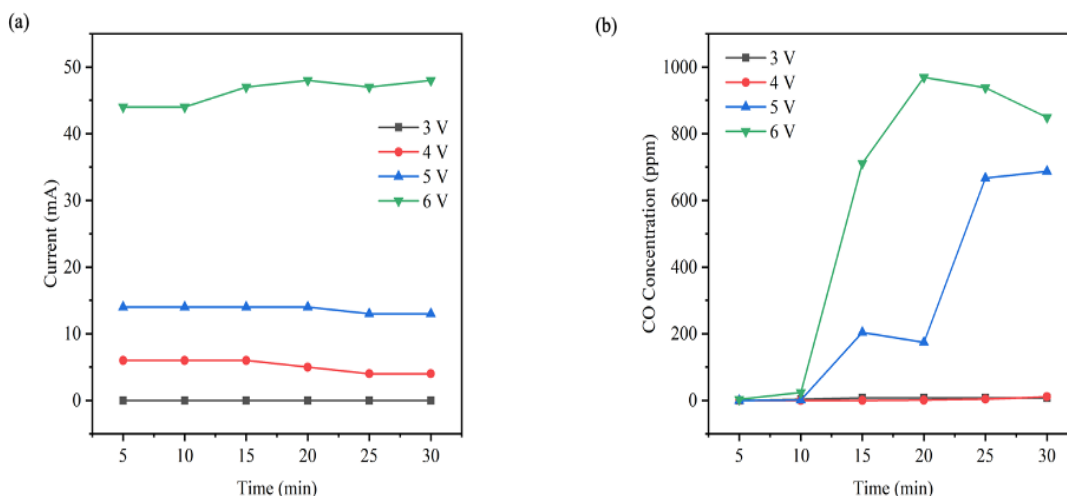
Figure 31 CO concentration (ppm) and current (mA) for CO_2 flow rate of 120 ml min^{-1}.

The sharply increasing of CO concentration at a high flow rate through porous cell could be describe by following scenarios: (1) The flowing CO_2 through packed-bed continuously removes CO from the felt pores releasing the CO from the catalyst surface, so that available active site for further CO_2 reduction. (2) The local pH in the felt pores is stable with fresh incoming CO_2. Thus, increasing in flow rate appears to be enhance mass transport of CO_2 reduction (57). Nevertheless, the effects of flow rate are need further investigations. The flow rate might against effects of enhancing mass transfer and due to short residence time at high flow rate. During the experiment of CO_2 reduction at 6 V with flow rate of 120 ml min^{-1}, water vapor was condensed in packed-bed leading to high current at this condition.

4.1.2 Two-cell bed reactor.

For two-cell bed reactor, both CO concentration and the current trends were consistency with increase applied voltage as shown in fig.32. The highest CO faradaic efficiency (12.43%) was observed at 11 V and 120 ml min^{-1}. This suggests that the optimum voltage for the CO selectivity is 11 V under the studied conditions. However, the effect of flow rate on CO_2 reduction in two-cell bed is inconclusive. The fluctuation of currents during the reduction was observed. The low currents compared to single-cell bed could be described by the deficiency of the water distribution. The water distribution within an electrochemical cell has impacted as a crucial factor in enhancing the CO_2 reduction performance. The presence of H_2O plays a significant role in improving the CO_2 reduction, such as increasing conductivity and proton donor (58) so that an unstable water distribution could lead to insufficient proton to complete the CO_2 reduction reaction.
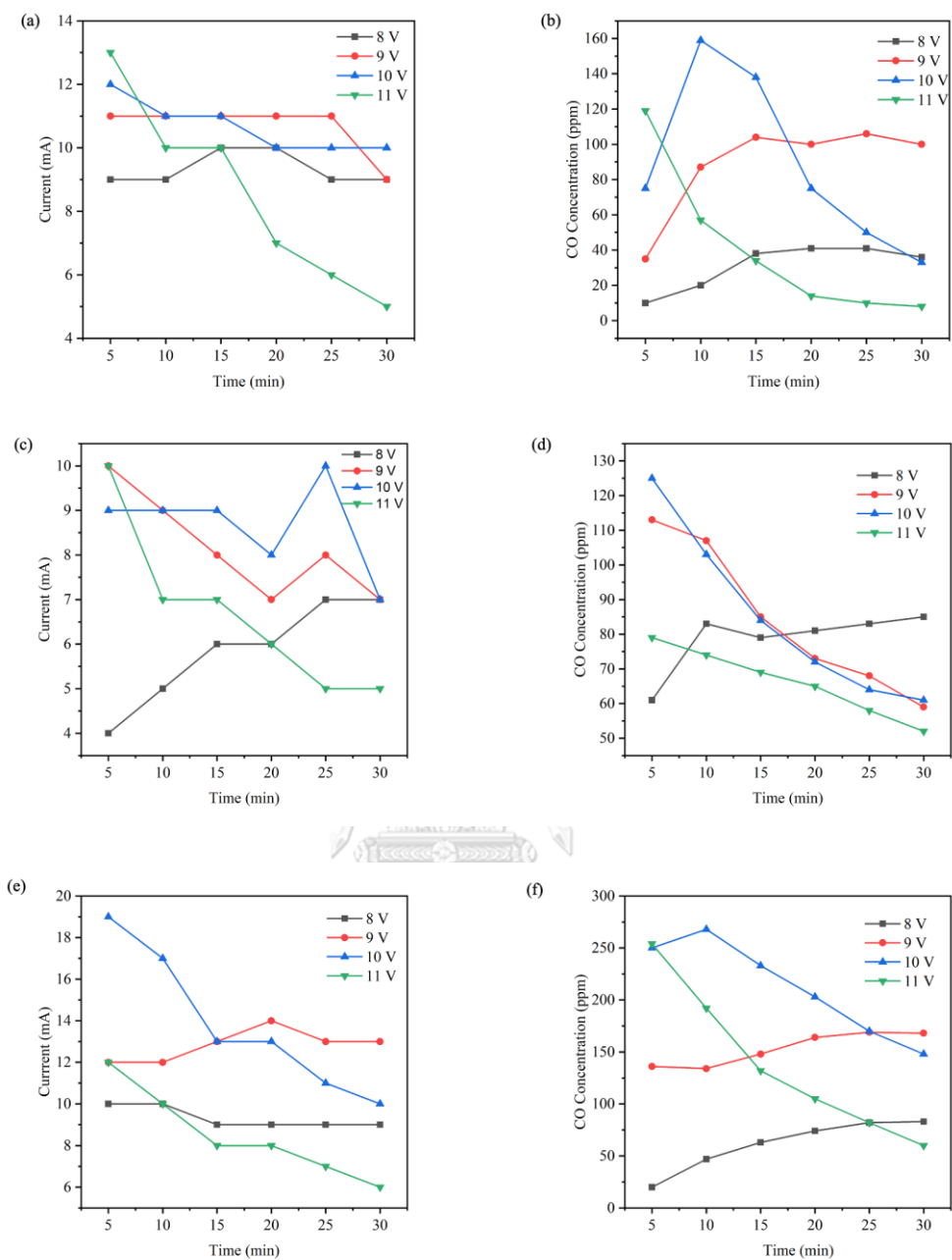
Figure 32 CO concentration (ppm) and current (mA) for CO_2 flow rate of 40 (a, b), 80 (c. d), and 120 ml min^{-1} (e, f) of a two-cell bed reactor.
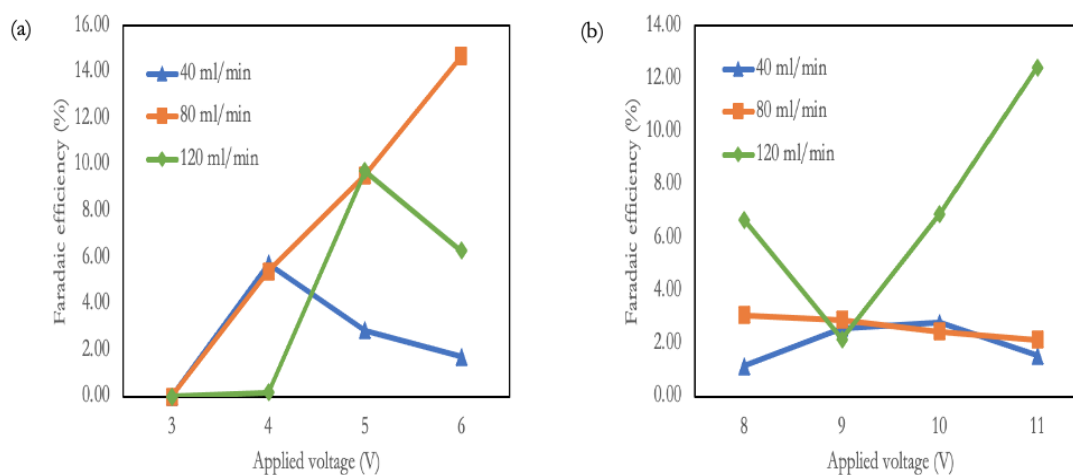
Figure 33 Faradaic efficiency of (a) a single-cell bed and (b) a two-cell bed.

4.2 Cell stability

The results presented in fig.34 fast deactivate after 30 minutes of operation in packed-bed reactor. A felt was analyzed after use by scanning electron microscopy (SEM). After 30 min of operation, both the current and the CO concentration gradually declined. Fig.34b, the degradation of the used felt was observed and might cause the deteriorating performance (59, 60). The SEM images showed a flaking scattered on carbon fibre surface after CO_2 reduction. Further, the short-term operation in the packed-bed might be involve the water management. The cell stability for CO_2 reduction to CO was controlled by water delivery along the cell where dehydration of the electrochemical cell could reduce CO_2 reduction performance. Otherwise, the perspiration rate could also cause hampers the CO_2 diffusion. The accumulation of water in packed-bed of 120 ml min^{-1} at 6 V (fig.30) was observed during the reaction so that accessibility of CO_2 to the felt active site was restricted (61). The excess water in packed-bed triggered water splitting which became main reaction instead of CO_2 reduction reaction caused unnecessary energy loss. Hence, the optimal humidify in CO_2 stream is one of the keys to maintain uniform current and electroreduction performance (62).

Besides, the bed porosity and thickness of packed-bed also suggest that mass transfer phenomena porosity between packed-bed might play a role in improved selectivity towards CO_2 electroreduction (63). The various patterns and designs including bed height, number of cell stack, and bed compact have impact on the diffusion of H_2O and CO_2 along the packed-bed. The nonuniform CO_2 and H_2O might contribute to fluctuation in current and CO concentration which complicated the cell performance analysis.
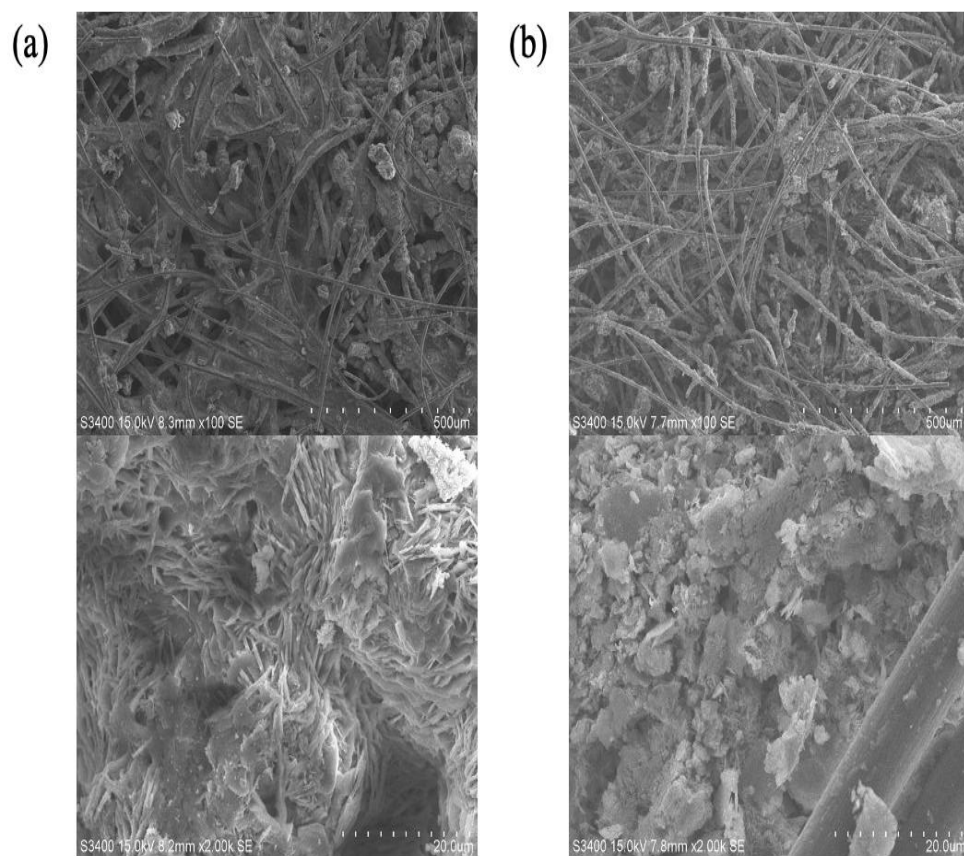
Figure 34 SEM analysis of (a) Zn deposited felt, and (b) a used Zn deposited carbon felt.

จุฬาลงกรณ์มหาวิทยาลัย

CHULALONGKORN UNIVERSITY

Chapter 5
Conclusions and Perspectives

Electrochemical packed-bed reactor for reducing CO_2 is being developed and was successfully converting CO_2 to CO. In this work, applied voltage and CO_2 flow rate was investigated on CO_2 reduction reaction in packed-bed reactor. An increasing in applied voltage increased the current and CO concentration for both single-cell configuration and two-cell configuration packed-bed reactor. Nevertheless, the effect of flowrates is still inconclusive. Increasing the flow rate might against effects of enhancing mass transfer because short residence time in the reactor. However, the two-cell bed reactor faced a water distribution problem, which decreased both the current and CO concentration. To modify the performance of our cell design, we have introduced several strategies for CO_2 reduction.

- Improvement the electrodeposition of Zn on carbon felt by adjusting the current.
- Solid porous polymer electrolyte membrane might be a clue for optimizing ion exchange, conductivity, and water transport.
- Varying time for NaOH absorption of the resin to efficiently capture CO_2.
- Optimized polymer loading to alleviate mass transfer limitation due to high compact of polymer.
- Controlling process parameters including humidity, flow rate, and pressure.

The investigations in this work are still at a primitive platform that require further commercial development and more variables need to be addressed which help to comprehend CO_2 electroreduction.

Appendix

Appendix A

Table 4 The effect of applied voltage on CO concentration at CO_2 flow rate of 40-, 80-, and 120-ml min^{-1} of a single-cell bed reactor.

Flow rate (ml min^{-1})	Time (min)	Current (mA)				CO concentration (ppm)			
		3 V	4 V	5 V	6V	3 V	4 V	5 V	6 V
40	5	0	6	13	23	0	173	400	697
	10	0	5	13	22	0	259	530	828
	15	0	5	12	24	0	249	492	711
	20	0	5	12	30	0	234	475	898
	25	0	4	12	31	0	220	460	643
	30	0	4	13	32	0	212	434	609
80	5	0	4	18	26	0	0	0	2
	10	0	4	16	24	0	0	1	3
	15	0	4	15	22	1	0	2	23
	20	0	4	14	22	2	23	329	1064
	25	0	4	14	21	4	11	679	1479
	30	0	4	14	21	5	184	1008	1825
120	5	0	6	14	44	0	0	0	3
	10	0	6	14	44	3	0	1	24
	15	0	6	14	47	8	0	204	711
	20	0	5	14	48	8	1	174	969
	25	0	4	13	47	8	4	667	938
	30	0	4	13	48	8	11	687	849

จุฬาลงกรณ์มหาวิทยาลัย

CHULALONGKORN UNIVERSITY

Table 5 The effect of applied voltage on CO concentration at CO_2 flow rate of 40-, 80-, and 120-ml min^{-1} of a two-cell bed reactor.

Flow rate (ml min^{-1})	Time (min)	Current (mA)				CO concentration (ppm)			
		8 V	9 V	10 V	11 V	8 V	9 V	10 V	11 V
40	5	9	11	12	13	10	35	75	119
	10	9	11	11	10	20	87	159	57
	15	10	11	11	10	38	104	138	34
	20	10	11	10	7	41	100	75	14
	25	9	11	10	6	41	106	50	10
	30	9	9	10	5	36	100	33	8
80	5	4	10	9	10	61	113	125	79
	10	5	9	9	7	83	107	103	74
	15	6	8	9	7	79	85	84	69
	20	6	7	8	6	81	73	72	65
	25	7	8	10	5	83	68	64	58
	30	7	7	7	5	85	59	61	52
120	5	10	12	19	12	20	136	250	254
	10	10	12	17	10	47	134	268	192
	15	9	13	13	6	63	148	233	132
	20	9	14	13	8	74	164	203	105
	25	9	13	11	7	82	169	170	82
	30	9	13	10	6	83	168	148	60

Appendix B

The faradaic efficiency in chapter 4 was calculated following the formula in section 2.1.2. Please note: Average current was substituted for this calculation, since current was observed nearly constant over time. The area of plot between CO concentration and time was obtained by Origin program.

Table 6 The area of graph CO concentration vs. time of 40, 80, and 120 ml min^{-1} of a single-cell bed reactor.

Flow rate (ml min^{-1})	Average current (mA)				Area (ppm min)			
	3 V	4 V	5 V	6 V	3 V	4 V	5 V	6 V
40	0	4.83	12.5	27	0	1447.5	1870	2430
80	0	4	15.17	22.67	47.5	1130	7565	17360
120	0	5.17	13.67	46.33	155	52.5	6945	15265

Table 7 The area of graph CO concentration vs. time of 40-, 80-, and 120-ml min^{-1} of a two-cell bed reactor.

Flow rate (ml min^{-1})	Average current (mA)				Area (ppm min)			
	8 V	9 V	10 V	11 V	8 V	9 V	10 V	11 V
40	9.33	10.67	10.67	8.5	565	1447.5	1555	692.5
80	5.83	8.17	8.67	6.67	470	620	555	375.5
120	9.33	12.83	13.83	8.5	1087.5	485	1665	1840

For example, calculate mole of CO at 6 V with CO_2 flow rate of 80 ml min^{-1} of a single-cell bed reactor.

$$\text{Mole of CO} = \frac{17360 \text{ mol CO} \times \text{min}}{10^6 \text{ mol CO2}} \times \frac{80 \text{ mL CO2}}{\text{min}} \times \frac{1 \text{ L CO2}}{1000 \text{ mL CO2}} \times \frac{1 \text{ mol CO2}}{22.4 \text{ L CO2}} = 3.10* 10^{-5}$$

$$Q = 22.67 \times 10^{-3} A \times 1800 \, s = 40.80 \text{ A s.}$$

$$FE = \frac{3.10 \times 10^5 \, mol \times 2 \times \frac{96,485 \, A \cdot s}{mol}}{40.8 \, A \cdot s} \times 100\% = 14.66\%$$

Table 8 Faradaic efficiency of a single-cell bed reactor and a two-cell bed reactor.

Flow rate (ml min^{-1})	A single-cell bed reactor				A two-cell bed reactor			
	3 V	4 V	5 V	6 V	8 V	9 V	10 V	11 V
40	-	5.73	2.86	1.72	1.16	2.6	2.79	1.56
80	-	5.41	9.55	14.66	3.08	2.91	2.45	2.16
120	-	0.19	9.73	6.31	6.69	2.17	6.91	12.43

REFERENCES

1.   Endrődi B, Bencsik G, Darvas F, Jones R, Rajeshwar K, Janáky C. Continuous-flow electroreduction of carbon dioxide. Progress in Energy and Combustion Science. 2017;62:133-54.

2.   Rogelj J, den Elzen M, Hohne N, Fransen T, Fekete H, Winkler H, et al. Paris Agreement climate proposals need a boost to keep warming well below 2 degrees C. Nature. 2016;534(7609):631-9.

3.   Albo J, Alvarez-Guerra M, Castaño P, Irabien A. Towards the electrochemical conversion of carbon dioxide into methanol. Green Chemistry. 2015;17(4):2304-24.

4.   Liu M, Yi Y, Wang L, Guo H, Bogaerts A. Hydrogenation of Carbon Dioxide to Value-Added Chemicals by Heterogeneous Catalysis and Plasma Catalysis. Catalysts. 2019;9(3).

5.   Avila-Bolivar B, Garcia-Cruz L, Montiel V, Solla-Gullon J. Electrochemical Reduction of CO2 to Formate on Easily Prepared Carbon-Supported Bi Nanoparticles. Molecules. 2019;24(11).

6.   Chang X, Wang T, Gong J. CO2 photo-reduction: insights into CO2 activation and reaction on surfaces of photocatalysts. Energy & Environmental Science. 2016;9(7):2177-96.

7.   Lorentzou S, Karagiannakis G, Pagkoura C, Zygogianni A, Konstandopoulos AG. Thermochemical CO2 and CO2/H2O Splitting over NiFe2O4 for Solar Fuels Synthesis. Energy Procedia. 2014;49:1999-2008.

8.   Dong B-X, Wang L-Z, Song L, Zhao J, Teng Y-L. Thermochemical Reduction of Carbon Dioxide with Alkali Metal Hydrides, Producing Methane and Hydrogen Fuels at Moderate Temperatures. Energy & Fuels. 2016;30(8):6620-5.

9.   Scibioh MA, Viswanathan B. Electrochemical Reduction of CO 2. Carbon Dioxide to Chemicals and Fuels2018. p. 307-71.

10.   Hori Y, Kikuchi K, Suzuki S. Production of CO and CH4 in electrochemical reduction of CO2 at metal electrodes in aqueous hydrogencarbonate solution. Chemistry Letters. 1985;14(11):1695-8.

11.   Chen Y, Li CW, Kanan MW. Aqueous CO2 reduction at very low overpotential on oxide-derived Au nanoparticles. J Am Chem Soc. 2012;134(49):19969-72.

12.   Li CW, Kanan MW. CO2 reduction at low overpotential on Cu electrodes resulting from the reduction of thick Cu2O films. J Am Chem Soc. 2012;134(17):7231-4.

13.   Irtem E, Andreu T, Parra A, Hernández-Alonso MD, García-Rodríguez S, Riesco-García JM, et al. Low-energy formate production from CO2 electroreduction using electrodeposited tin on GDE. Journal of

Materials Chemistry A. 2016;4(35):13582-8.

14. Olivo A, Ghedini E, Signoretto M, Compagnoni M, Rossetti I. Liquid vs. Gas Phase CO2 Photoreduction Process: Which Is the Effect of the Reaction Medium? Energies. 2017;10(9).

15. Sánchez OG, Birdja YY, Bulut M, Vaes J, Breugelmans T, Pant D. Recent advances in industrial CO2 electroreduction. Current Opinion in Green and Sustainable Chemistry. 2019;16:47-56.

16. Zhong H, Fujii K, Nakano Y, Jin F. Effect of CO2 Bubbling into Aqueous Solutions Used for Electrochemical Reduction of CO2 for Energy Conversion and Storage. The Journal of Physical Chemistry C. 2014;119(1):55-61.

17. Chandrasekaran K, Bockris LM. In-situ spectroscopic investigation of adsorbed intermediate radicals in electrochemical reactions: CO2− on platinum. Surface science. 1987;185(3):495-514.

18. Schneider J, Jia H, Muckerman JT, Fujita E. Thermodynamics and kinetics of CO2, CO, and H+ binding to the metal centre of CO2 reduction catalysts. Chem Soc Rev. 2012;41(6):2036-51.

19. Jitaru M, Lowy D, Toma M, Toma B, Oniciu L. Electrochemical reduction of carbon dioxide on flat metallic cathodes. Journal of Applied Electrochemistry. 1997;27(8):875-89.

20. Hori Yi. Electrochemical CO 2 reduction on metal electrodes. Modern aspects of electrochemistry: Springer; 2008. p. 89-189.

21. Lee M-Y, Park KT, Lee W, Lim H, Kwon Y, Kang S. Current achievements and the future direction of electrochemical CO2 reduction: A short review. Critical Reviews in Environmental Science and Technology. 2019;50(8):769-815.

22. Song J, Song H, Kim B, Oh J. Towards Higher Rate Electrochemical CO2 Conversion: From Liquid-Phase to Gas-Phase Systems. Catalysts. 2019;9(3).

23. Noda H, Ikeda S, Yamamoto A, Einaga H, Ito K. Kinetics of Electrochemical Reduction of Carbon Dioxide on a Gold Electrode in Phosphate Buffer Solutions. Bulletin of the Chemical Society of Japan. 1995;68(7):1889-95.

24. Nursanto EB, Jeon HS, Kim C, Jee MS, Koh JH, Hwang YJ, et al. Gold catalyst reactivity for CO2 electro-reduction: From nano particle to layer. Catalysis Today. 2016;260:107-11.

25. Peterson AA, Nørskov JK. Activity Descriptors for CO2 Electroreduction to Methane on Transition-Metal Catalysts. The Journal of Physical Chemistry Letters. 2012;3(2):251-8.

26. Hatsukade T, Kuhl KP, Cave ER, Abram DN, Jaramillo TF. Insights into the electrocatalytic reduction of CO(2) on metallic silver surfaces.

Phys Chem Chem Phys. 2014;16(27):13814-9.

27. Kortlever R, Shen J, Schouten KJ, Calle-Vallejo F, Koper MT. Catalysts and Reaction Pathways for the Electrochemical Reduction of Carbon Dioxide. J Phys Chem Lett. 2015;6(20):4073-82.

28. Firet NJ, Smith WA. Probing the Reaction Mechanism of CO2 Electroreduction over Ag Films via Operando Infrared Spectroscopy. ACS Catalysis. 2016;7(1):606-12.

29. Ma M, Trzesniewski BJ, Xie J, Smith WA. Selective and Efficient Reduction of Carbon Dioxide to Carbon Monoxide on Oxide-Derived Nanostructured Silver Electrocatalysts. Angew Chem Int Ed Engl. 2016;55(33):9748-52.

30. Luo W, Zhang J, Li M, Züttel A. Boosting CO Production in Electrocatalytic CO2 Reduction on Highly Porous Zn Catalysts. ACS Catalysis. 2019;9(5):3783-91.

31. Rosen J, Hutchings GS, Lu Q, Forest RV, Moore A, Jiao F. Electrodeposited Zn Dendrites with Enhanced CO Selectivity for Electrocatalytic CO2Reduction. ACS Catalysis. 2015;5(8):4586-91.

32. Konig M, Vaes J, Klemm E, Pant D. Solvents and Supporting Electrolytes in the Electrocatalytic Reduction of CO2. iScience. 2019;19:135-60.

33. Bumroongsakulsawat P, Kelsall GH. Effect of solution pH on CO: formate formation rates during electrochemical reduction of aqueous CO2 at Sn cathodes. Electrochimica Acta. 2014;141:216-25.

34. Lu Q, Rosen J, Zhou Y, Hutchings GS, Kimmel YC, Chen JG, et al. A selective and efficient electrocatalyst for carbon dioxide reduction. Nat Commun. 2014;5:3242.

35. Lee J, Lim J, Roh C-W, Whang HS, Lee H. Electrochemical CO2 reduction using alkaline membrane electrode assembly on various metal electrodes. Journal of CO2 Utilization. 2019;31:244-50.

36. Li YC, Yan Z, Hitt J, Wycisk R, Pintauro PN, Mallouk TE. Bipolar Membranes Inhibit Product Crossover in CO2
 Electrolysis Cells. Advanced Sustainable Systems. 2018;2(4).

37. Whipple DT, Finke EC, Kenis PJA. Microfluidic Reactor for the Electrochemical Reduction of Carbon Dioxide: The Effect of pH. Electrochemical and Solid-State Letters. 2010;13(9).

38. Gabardo CM, Seifitokaldani A, Edwards JP, Dinh C-T, Burdyny T, Kibria MG, et al. Combined high alkalinity and pressurization enable efficient CO2 electroreduction to CO. Energy & Environmental Science. 2018;11(9):2531-9.

39. Ye L, Zhang M, Huang P, Guo G, Hong M, Li C, et al. Enhancing CO2 electrolysis through synergistic control of non-stoichiometry and

doping to tune cathode surface structures. Nat Commun. 2017;8:14785.

40. Ebbesen SD, Knibbe R, Mogensen M. Co-Electrolysis of Steam and Carbon Dioxide in Solid Oxide Cells. Journal of The Electrochemical Society. 2012;159(8):F482-F9.

41. Liang S, Altaf N, Huang L, Gao Y, Wang Q. Electrolytic cell design for electrochemical CO2 reduction. Journal of CO2 Utilization. 2020;35:90-105.

42. Hori Y, Ito H, Okano K, Nagasu K, Sato S. Silver-coated ion exchange membrane electrode applied to electrochemical reduction of carbon dioxide. Electrochimica Acta. 2003;48(18):2651-7.

43. Ampelli C, Genovese C, Perathoner S, Centi G, Errahali M, Gatti G, et al. An electrochemical reactor for the CO2 reduction in gas phase by using conductive polymer based electrocatalysts. Chemical Engineering Transactions. 2014;41:13-8.

44. Wu J, Sharma PP, Harris BH, Zhou X-D. Electrochemical reduction of carbon dioxide: IV dependence of the Faradaic efficiency and current density on the microstructure and thickness of tin electrode. Journal of Power Sources. 2014;258:189-94.

45. Hou P, Wang X, Wang Z, Kang P. Gas Phase Electrolysis of Carbon Dioxide to Carbon Monoxide Using Nickel Nitride as the Carbon Enrichment Catalyst. ACS Appl Mater Interfaces. 2018;10(44):38024-31.

46. Wang G, Pan J, Jiang SP, Yang H. Gas phase electrochemical conversion of humidified CO2 to CO and H2 on proton-exchange and alkaline anion-exchange membrane fuel cell reactors. Journal of CO2 Utilization. 2018;23:152-8.

47. Kim B, Ma S, Molly Jhong H-R, Kenis PJA. Influence of dilute feed and pH on electrochemical reduction of CO2 to CO on Ag in a continuous flow electrolyzer. Electrochimica Acta. 2015;166:271-6.

48. Yang H, Kaczur JJ, Sajjad SD, Masel RI. Electrochemical conversion of CO2 to formic acid utilizing Sustainion™ membranes. Journal of CO2 Utilization. 2017;20:208-17.

49. Delacourt C, Ridgway PL, Kerr JB, Newman J. Design of an Electrochemical Cell Making Syngas (CO+H[sub 2]) from CO[sub 2] and H[sub 2]O Reduction at Room Temperature. Journal of The Electrochemical Society. 2008;155(1).

50. Verma S, Hamasaki Y, Kim C, Huang W, Lu S, Jhong H-RM, et al. Insights into the Low Overpotential Electroreduction of CO2 to CO on a Supported Gold Catalyst in an Alkaline Flow Electrolyzer. ACS Energy Letters. 2017;3(1):193-8.

51. Dufek EJ, Lister TE, Stone SG, McIlwain ME. Operation of a Pressurized System for Continuous Reduction of CO2. Journal of The

Electrochemical Society. 2012;159(9):F514-F7.

52. Köleli F, Balun D. Reduction of CO2 under high pressure and high temperature on Pb-granule electrodes in a fixed-bed reactor in aqueous medium. Applied Catalysis A: General. 2004;274(1-2):237-42.

53. Köleli F, Yeşilkaynak T, Balun Kayan D. High pressure-high temperature CO2 electro-reduction on Sn granules in a fixed-bed reactor. Fresenius Environmental Bulletin. 2003;12:1202-6.

54. Monroe MM, Lobaccaro P, Lum Y, Ager JW. Membraneless laminar flow cell for electrocatalytic CO2 reduction with liquid product separation. Journal of Physics D: Applied Physics. 2017;50(15).

55. Ahangari HT, Portail T, Marshall AT. Comparing the electrocatalytic reduction of CO2 to CO on gold cathodes in batch and continuous flow electrochemical cells. Electrochemistry Communications. 2019;101:78-81.

56. Dufek EJ, Lister TE, McIlwain ME. Bench-scale electrochemical system for generation of CO and syn-gas. Journal of Applied Electrochemistry. 2011;41(6):623-31.

57. Vedharathinam V, Qi Z, Horwood C, Bourcier B, Stadermann M, Biener J, et al. Using a 3D Porous Flow-Through Electrode Geometry for High-Rate Electrochemical Reduction of CO2 to CO in Ionic Liquid. ACS Catalysis. 2019;9(12):10605-11.

58. Shi J, Shen F-x, Shi F, Song N, Jia Y-J, Hu Y-Q, et al. Electrochemical reduction of CO2 into CO in tetrabutylammonium perchlorate/propylene carbonate: Water effects and mechanism. Electrochimica Acta. 2017;240:114-21.

59. Nibel O, Taylor S, Beard Patru A, Fabbri E, Gubler L, Schmidt T. Performance of Different Carbon Electrode Materials: Insights into Stability and Degradation under Real Vanadium Redox Flow Battery Operating Conditions. Journal of The Electrochemical Society. 2017;164:A1608-A15.

60. Derr I, Bruns M, Langner J, Fetyan A, Melke J, Roth C. Degradation of all-vanadium redox flow batteries (VRFB) investigated by electrochemical impedance and X-ray photoelectron spectroscopy: Part 2 electrochemical degradation. Journal of Power Sources. 2016;325:351-9.

61. Duarte M, De Mot B, Hereijgers J, Breugelmans T. Electrochemical Reduction of CO
2
: Effect of Convective CO
2
Supply in Gas Diffusion Electrodes. ChemElectroChem. 2019;6(22):5596-602.

62. Weekes DM, Salvatore DA, Reyes A, Huang A, Berlinguette CP.

Electrolytic CO2 Reduction in a Flow Cell. Acc Chem Res. 2018;51(4):910-8.

63. Kas R, Hummadi KK, Kortlever R, de Wit P, Milbrat A, Luiten-Olieman MW, et al. Three-dimensional porous hollow fibre copper electrodes for efficient and high-rate electrochemical carbon dioxide reduction. Nat Commun. 2016;7:10748.

VITA

NAME	Suwakul Chaiwarit
DATE OF BIRTH	23 November 1995
PLACE OF BIRTH	Chiangrai
INSTITUTIONS ATTENDED	Faculty of engineering, Chemical engineering department, Mahidol university. (Bachelor's degree)
HOME ADDRESS	305, Moo 3, Baan doo, Mueang, Chiangrai, Thailand, 57100.

จุฬาลงกรณ์มหาวิทยาลัย
CHULALONGKORN UNIVERSITY